ASTROBIOLOGY
Volume 20, Number 4, 2020
Mary Ann Liebert, Inc.
DOI: 10.1089/ast.2019.2044

The Case for Ancient Hot Springs in Gusev Crater, Mars

Steven W. Ruff,[1] Kathleen A. Campbell,[2] Martin J. Van Kranendonk,[3] Melissa S. Rice,[4] and Jack D. Farmer[1]

Abstract

The origin and age of opaline silica deposits discovered by the Spirit rover adjacent to the Home Plate feature in the Columbia Hills of Gusev crater remains debated, in part because of their proximity to sulfur-rich soils. Processes related to fumarolic activity and to hot springs and/or geysers are the leading candidates. Both processes are known to produce opaline silica on Earth, but with differences in composition, morphology, texture, and stratigraphy. Here, we incorporate new and existing observations of the Home Plate region with observations from field and laboratory work to address the competing hypotheses. The results, which include new evidence for a hot spring vent mound, demonstrate that a volcanic hydrothermal system manifesting both hot spring/geyser and fumarolic activity best explains the opaline silica rocks and proximal S-rich materials, respectively. The opaline silica rocks most likely are sinter deposits derived from hot spring activity. Stratigraphic evidence indicates that their deposition occurred before the emplacement of the volcaniclastic deposits comprising Home Plate and nearby ridges. Because sinter deposits throughout geologic history on Earth preserve evidence for microbial life, they are a key target in the search for ancient life on Mars. Key Words: Mars—Opaline silica—Hot springs—Sinter—Columbia Hills—Astrobiology. Astrobiology 20, 475–499.

1. Introduction

In 2007, the Mars Exploration Rover Spirit encountered rocks and regolith composed of opaline silica (amorphous $SiO_2 \cdot nH_2O$) next to a volcanic landform dubbed Home Plate in the Columbia Hills of Gusev crater (Squyres *et al.*, 2008). The origin and age of the opaline silica have been the subject of debate ever since. Two silica-forming processes have been suggested, one involving leaching of existing materials in the landscape by acid-sulfate condensates arising from volcanic fumaroles, and the other involving direct precipitation of opaline silica from hot spring and/or geyser fluids (e.g., Squyres *et al.*, 2008; Yen *et al.*, 2008; Ruff *et al.*, 2011). Both processes occur in volcanic hydrothermal settings, the presence of which is indicated in the Columbia Hills by evidence for hydrovolcanism and by geochemical and mineralogic indicators of hydrothermal fluids (e.g., Squyres *et al.*, 2007, 2008; Lewis *et al.*, 2008; Schmidt *et al.*, 2008, 2009; Wang *et al.*, 2008; Yen *et al.*, 2008).

On Earth, the expression of opaline silica arising from these two processes is markedly different, manifested by differences in composition, morphology, texture, and stratigraphy, which are, in part, a function of the role of microbial constituents. Neglecting any of these characteristics can lead to misidentification of process, which precludes the proper assessment of habitability and microbial preservation potential of the setting, a key objective in Mars exploration, as well as in the investigation of life on early Earth.

Fumarolic acid-sulfate leaching occurs where sulfuric acid aerosols (H_2SO_4), produced from oxidation and hydration of volcanic gases, condense onto materials surrounding fumaroles (e.g., Payne and Mau, 1946; Bignall and Browne, 1994; Rodgers *et al.*, 2002). Where silicate materials are present, leaching removes cations and passively enriches silica, leaving a residue of opaline silica that ranges from millimeter-scale coatings to complete mineral replacement of existing rocks. Fumarolic settings host microbial communities (e.g., Ellis *et al.*, 2008; Costello *et al.*, 2009; Benson *et al.*, 2011; Cockell *et al.*, 2019), but to our knowledge, their preservation over geological timescales has not been documented.

In contrast, where hot silica-rich waters emanating from hot springs and geysers cool and evaporate, they precipitate opaline silica on any available surface, accumulating as sheet-like chemical sedimentary deposits known as sinter. Most sinter deposits are produced from near-neutral pH alkali chloride springs, with accumulations that are

[1]School of Earth and Space Exploration, Arizona State University, Tempe, Arizona.
[2]School of Environment and Te Ao Mārama—Centre for Fundamental Inquiry, The University of Auckland, Auckland, New Zealand.
[3]Australian Centre for Astrobiology, School of Biological, Earth and Environmental Sciences, University of New South Wales Sydney, Sydney, Australia.
[4]Department of Geology, Western Washington University, Bellingham, Washington.

centimeters to meters thick, but acid-sulfate-chloride springs with pH as low as 2.1 are also known to produce sinter deposits (Schinteie *et al.*, 2007). Because hot springs commonly host extensive microbial communities, the role of microbes in facilitating silica precipitation has long been debated (e.g., Weed, 1889; Allen, 1934; White *et al.*, 1956; Walter *et al.*, 1972) and continues to be investigated (e.g., personal communication; Tobler *et al.*, 2008; Orange *et al.*, 2013; Murphy *et al.*, personal communication). The potential for sinter deposits to entomb and preserve biomaterials and textures over geological timescales is well documented (e.g., Campbell *et al.*, 2019; Campbell *et al.*, 2001; Djokic *et al.*, 2017; Guido *et al.*, 2010; Rice *et al.*, 1995; Teece *et al.*, 2020 in this issue; Walter *et al.*, 1996; White *et al.*, 1989), which is a primary reason that they are a favored target in the search for ancient life on Mars (e.g., Walter and Des Marais, 1993; Farmer and Des Marais, 1999; Cady *et al.*, 2018).

The presence of sulfur-rich, fine-particulate regolith (S-rich ''soils'') in the Columbia Hills, some of which include silica enrichments, has been attributed to fumarolic activity and tied to the origin of the Home Plate opaline silica deposits based largely on compositional considerations and proximity (e.g., Squyres *et al.*, 2008; Wang *et al.*, 2008; Yen *et al.*, 2008). However, it has been shown recently that the ratio of Si to Ti compared with Si abundance is inconsistent with an acid leaching origin for some of the opaline silica rocks at Home Plate (Yen *et al.*, 2019). A range of other available observations also must be considered to resolve the ambiguity between identification of silica sinter and silica residue for the Home Plate opaline silica occurrence. Following on from the work of Ruff *et al.* (2011), we incorporate new and existing observations of the Home Plate region with observations from field and laboratory work to address this ambiguity. The results demonstrate that a volcanic hydrothermal system manifesting both hot spring/geyser and fumarolic activity best explains Home Plate silica deposits and nearby S-rich soils. The co-occurrence of these hydrothermal manifestations has long been recognized on Earth (e.g., Day and Allen, 1925; White, 1957; Ellis and Mahon, 1964; Sorey *et al.*, 1991; Bignall and Browne, 1994; McHenry *et al.*, 2017) and likely also occurred in ancient hydrothermal systems on Mars.

2. Background

2.1. Columbia Hills geological context

2.1.1. Geology. The Columbia Hills is a set of low hills rising up to $\sim$100 m above the surrounding plains, with a lateral extent of $\sim$6 km. From orbital images, it is apparent that the hills are embayed by the basaltic lava flows over which the Spirit rover traversed on its approach from the west (Fig. 1). The hills thus represent a kipuka, that is, an older terrain embayed by lava flows, one of many examples on the floor of Gusev crater. The embaying basaltic lava flows have been dated to $\sim$3.65 Ga based on crater retention age (Greeley *et al.*, 2005), which indicates that the terrain units comprising the Columbia Hills are older than this age. None of these terrain units is recognized elsewhere in Gusev to be present on top of the basaltic plains, although other kipukas appear to host comparable terrain units (Ruff *et al.*, 2014), supporting the idea that all of the Columbia Hills terrains are older than the embaying lava plains.

Spirit encountered a diversity of rock types along its traverse through the Columbia Hills, all of which appear to result from intrusive or extrusive magmas, explosive volcanic eruptions, or impact processes (e.g., Ruff *et al.*, 2006; Squyres *et al.*, 2006; Arvidson *et al.*, 2008, 2010; McSween *et al.*, 2008). No sedimentary rocks produced in a lake environment were encountered. This is contrary to expectation based on geomorphic evidence that Gusev crater once hosted a lake, one of the reasons that it was selected as the Spirit landing site (Squyres *et al.*, 2004). However, there are multiple examples indicative of the role of water in altering rocks both on the plains and in the Columbia Hills (e.g., Haskin *et al.*, 2005; Hurowitz *et al.*, 2006; Ming *et al.*, 2006; Clark *et al.*, 2007; Morris *et al.*, 2010; Ruff and Hamilton, 2017), including the possible role of lacustrine processes (Ruff *et al.*, 2014). Thus, there is abundant evidence for alteration by water in multiple places at multiple times in the geological history of Gusev crater.

All of the rock units explored by Spirit in the vicinity of Home Plate, with the exception of the opaline silica outcrops, appear to be volcanically derived materials of basaltic composition that are altered to varying degrees. Stratigraphic relationships are clearly expressed in some cases but ambiguous in others, as described herein. A conceptual model of the stratigraphic relationship of the opaline silica outcrops with other rock units is presented in Section 4.3. The stratigraphically lowest recognized unit, known as Halley class, is fine-grained, light-toned bedrock with a commonly platy outcrop expression. It is interpreted to be an ash deposit altered under oxidizing acid-sulfate-dominated conditions (Ming *et al.*, 2008; Squyres *et al.*, 2008). Found exclusively to the east and south of Home Plate, it is the only recognized rock unit in contact with outcrops of opaline silica (Squyres *et al.*, 2008).

The rocks of the Home Plate feature, an erosional remnant of volcaniclastic deposits up to a few meters thick and $\sim$80 m wide (Fig. 2), appear to be stratigraphically above the Halley class outcrops, although no direct contact is evident. The coarser-grained lower portion of Home Plate known as Barnhill class likely was emplaced by explosive volcanic activity and the finer-grained, cross-bedded upper portion known as Pesapallo (sub)class may represent either Aeolian reworking of the lower unit (Squyres *et al.*, 2007) or a pyroclastic surge deposit (Lewis *et al.*, 2008). Other candidates for Home Plate-like volcaniclastic deposits are present elsewhere within the Inner Basin of the Columbia Hills, identified by similar morphology and albedo characteristics (Rice *et al.*, 2010a). This suggests a more extensive and perhaps formerly continuous deposit of comparable pyroclastic materials (Fig. 1). A candidate volcanic vent dubbed Goddard, which may be the source of this material, is present $\sim$170 m to the south of the center of Home Plate (Rice *et al.*, 2010a) (Fig. 1). It was an intended target of exploration for Spirit but was not reached before the rover became embedded in fine particulate regolith, which precluded further driving (Arvidson *et al.*, 2010).

Lying above the Halley class rocks are two different layered rock units known as Torquas and Graham Land that are present on Mitcheltree Ridge to the east and Low Ridge to the south of Home Plate, respectively (Fig. 2). Both of these units host abundant, close-packed, millimeter-sized spherical grains that constitute possible volcanic accretionary lapilli (Arvidson *et al.*, 2008; Squyres *et al.*, 2008). Although their stratigraphic position above Halley class

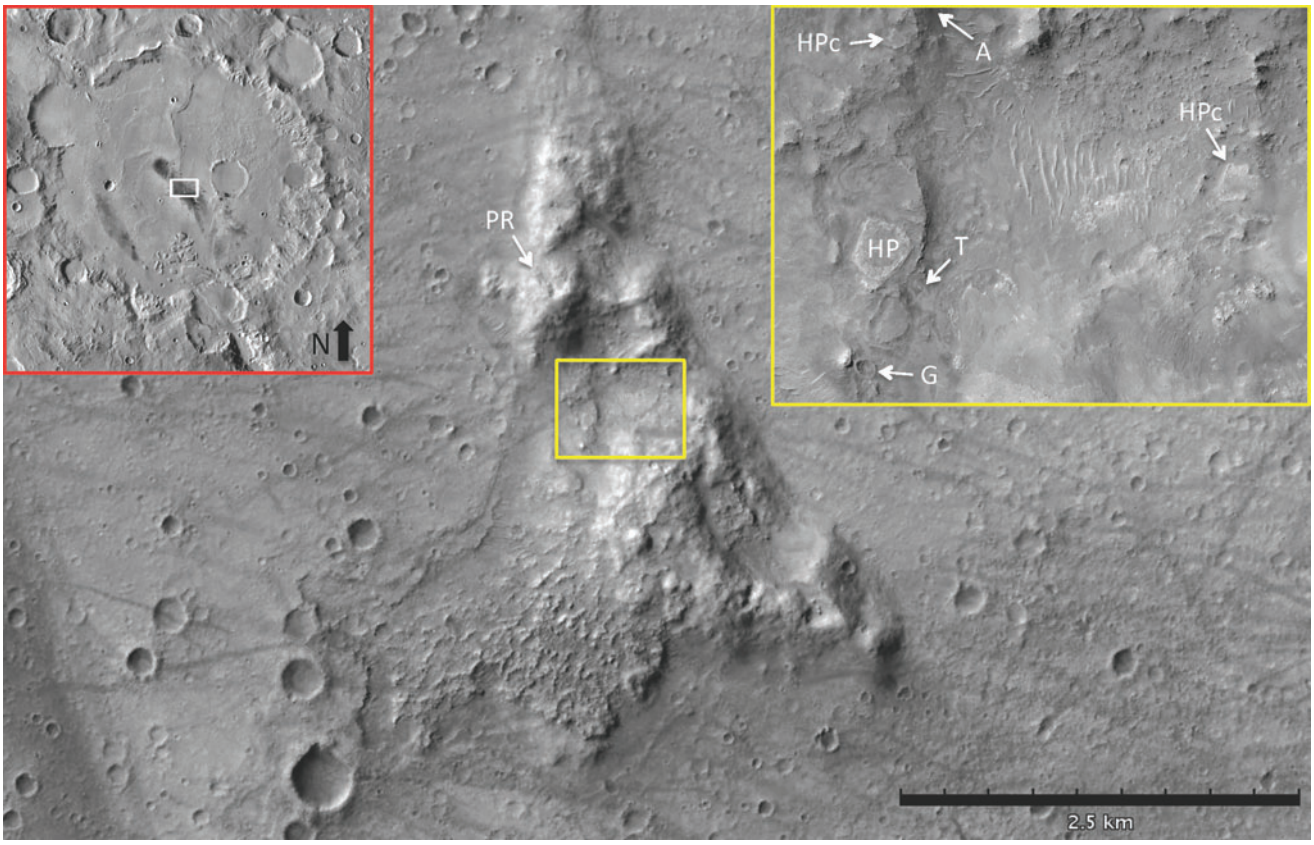

FIG. 1. Context of the Columbia Hills in Gusev crater. Red-lined inset image depicts the ~160 km diameter Gusev crater in a mosaic of THEMIS VIS images. The white rectangle (centered at 175.5° E, 14.6° S) is the location of the Columbia Hills shown in the main image, which is cropped from CTX B01_010098_1653_XI_14S184W. Basaltic lava flows have embayed the terrains of the Columbia Hills, implying that they are older than the flows. PR indicates Paso Robles S-rich soil. Yellow rectangle represents the yellow-lined inset image of the Inner Basin (cropped from HiRISE PSP_001513_1655_RED), which contains the Home Plate feature (HP) and two candidates for other Home Plate-like deposits (HPc), and the candidate volcanic vent feature called Goddard (G). Other S-rich soils are indicated at A for Arad and T for Tyrone. CTX, Context Camera; HiRISE, High-Resolution Imaging Science Experiment; THEMIS VIS, Thermal Emission Imaging System Visible Imaging System.

outcrops is clearly expressed, their relationship to Home Plate volcaniclastic rocks is not. They may be coeval but spatially separated deposits, perhaps originally interfingered, or they may be separated in time with intervening erosion, as suggested by the fact that the Home Plate rocks are moderately dipping, whereas the Torquas and Graham Land rocks are subhorizontal. Faulting is another possible explanation for the different orientations and distributions of what are otherwise compositionally relatively similar volcaniclastic rock units across the Eastern Valley (Fig. 2).

Capping all of these volcaniclastic rocks is a vesicular basaltic unit known as Irvine class, which occurs as cobbles and boulders on Mitcheltree and Low ridges, and as scattered blocks on top of Home Plate. These rocks may represent either disaggregated lava flows or scoria accumulations (Schmidt *et al.*, 2008).

2.1.2. Hydrothermal activity. There are multiple lines of evidence suggesting past hydrothermal activity in the vicinity of Home Plate and elsewhere within the portion of the Columbia Hills explored by Spirit. Sulfur-rich soil was observed on the north side of Husband Hill in regolith exposed by rover wheel disturbances. Dubbed Paso Robles, this material represents the type example for comparable S-rich soils encountered in a similar context closer to Home Plate (Fig. 1) (Yen *et al.*, 2008; Arvidson *et al.*, 2010) and perhaps elsewhere (Wang *et al.*, 2008; Winchell and Rice, 2017). All are light-toned soils, some with a yellowish hue, exposed by the rover's wheels from beneath darker basaltic soil. They are dominated by ferric iron sulfates, silica, and Mg-sulfates, one or more of which are hydrated, with indications of Ca-sulfates, Ca-phosphates, and other minor phases in some places (Campbell *et al.*, 2008; Wang *et al.*, 2008; Yen *et al.*, 2008). Some combination of volcanic vapors and acidic hydrothermal fluids is believed to be responsible for this material.

Hydrothermal alteration of Home Plate Barnhill class rocks is indicated by comparing their composition with that of the overlying Irvine class rocks, which may represent the unaltered, juvenile basaltic precursor composition (Schmidt *et al.*, 2008). Such comparisons demonstrate excess halogen and volatile siderophile elements in Barnhill class. This has been interpreted as evidence for brine addition during phreatomagmatic fragmentation that was later overprinted by hydrothermal alteration (Schmidt *et al.*, 2008). In this model, briny groundwater may have been the trigger fluid that

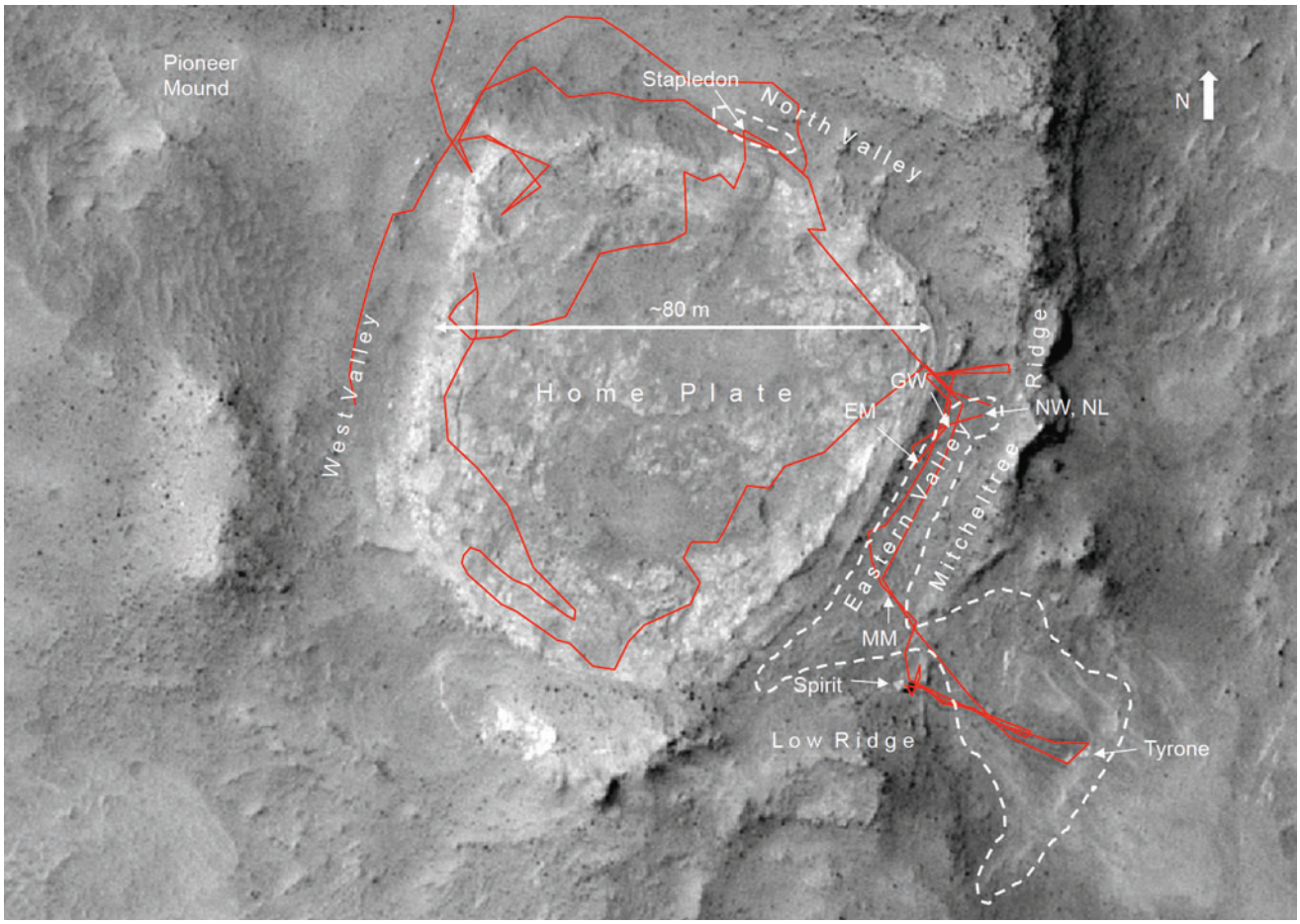

FIG. 2. Context of the Home Plate feature and opaline silica occurrences (modified from Ruff *et al.*, 2011). Dashed lines indicate approximate extent of recognized and likely silica-rich outcrops. Red line approximates rover traverse route reconstructed from wheel tracks seen in HiRISE and rover-based images. Opaline silica materials referred to in the text are: Gertrude Weise soil (GW), Elizabeth Mahon (EM) and Milltown Malbay (MM) nodules with digitate structures, and Nancy Warren (NW) and Norma Luker (NL) rocks with breccia texture. Other named features are described in the text. Image cropped from HiRISE PSP_001513_1655_RED.

initiated the phreatomagmatic eruption that formed the materials composing Home Plate and other associated features.

The presence of opaline silica around the margins of the Home Plate feature, in what clearly is a volcanic setting, strongly implies hydrothermal activity. Its proximity to the Paso Robles class S-rich soils and the Barnhill class rocks of Home Plate has been used to support the hypothesis of hydrothermal activity in those locations (e.g., Schmidt *et al.*, 2008, 2009; Yen *et al.*, 2008). Characteristics of the opaline silica occurrence are presented in the next section.

2.2. Opaline silica at Home Plate

Previous work has thoroughly documented the characteristics of the opaline silica occurrences adjacent to Home Plate (Squyres *et al.*, 2008; Ruff *et al.*, 2011; Ruff and Farmer, 2016), which are summarized here. Previously unpublished observations are presented in Section 4.

All of the known opaline silica occurrences are found within $\sim$50 m of the Home Plate feature around its north and east sides (Fig. 2). The silica displays what was described previously as a ''nodular'' appearance (Squyres *et al.*, 2008), indicating the generally rounded or bulbous morphology of the typically clustered pieces of light-toned rocks, which individually are mostly <15 cm in size (Fig. 3). No bedrock expression is evident, yet the rubbly appearing nodular silica resisted deformation from the rover wheels in multiple places along its traverse, leading to the descriptor ''outcrop.'' The lack of commingling of silica nodules with other rock types adds to the evidence that they are in-place outcrop rather than transported detritus. This homogeneity is especially recognizable because of the lighter tone and reddish to whitish hues of the nodular silica versus darker, bluer rocks of basaltic composition seen in false color images in the vicinity of Home Plate.

Discontinuous, low profile (<30 cm) nodular silica outcrops commonly occur directly on top of Halley class bedrock, which has a buff color and platy morphology that is quite distinct from the silica (Fig. 3). This contact relationship and topography-conforming expression contributes to the characterization of the silica outcrops as stratiform (Ruff *et al.*, 2011). No other contact relationship has been found, although silica outcrops were observed with no exposed lower contact. There is no obvious preferred orientation among the individual outcrops, which typically are a meter or two in length in their long dimension.

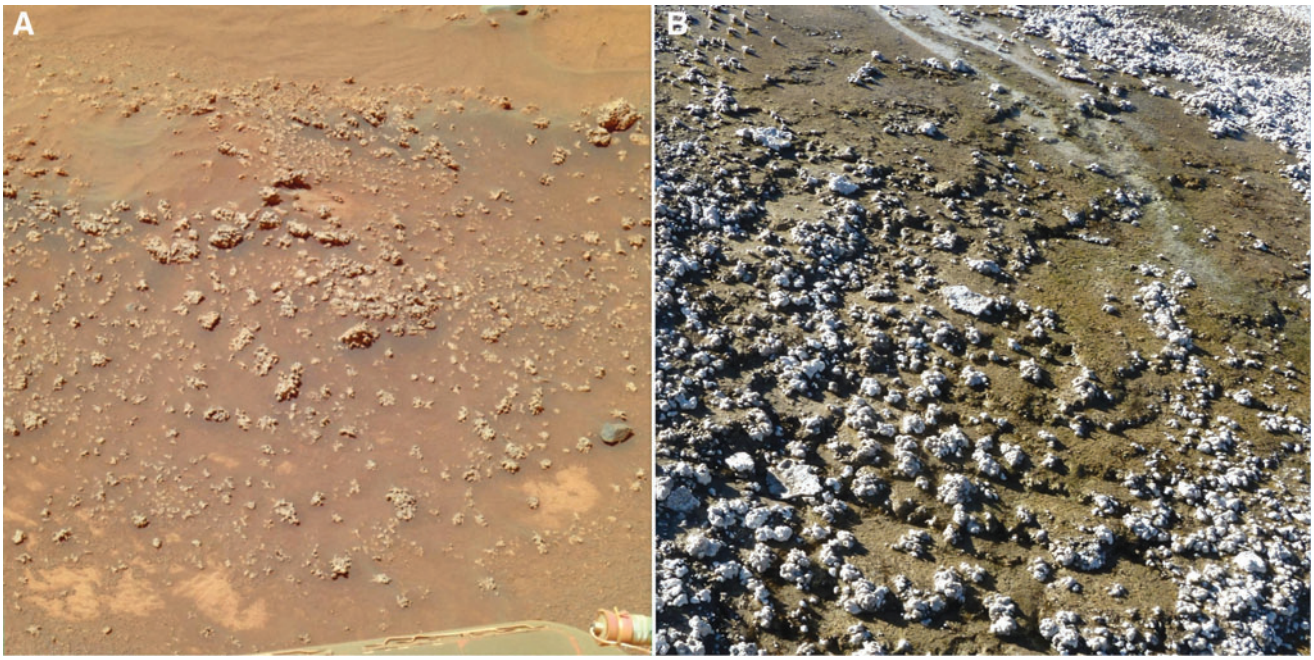

FIG. 3. Nodular opaline silica with digitate structures. **(A)** An example known as Milltown-Malbay shows some of the characteristics of the opaline silica outcrops adjacent to Home Plate (see Fig. 2 for context) in this Pancam approximate true color image (sol 778, P2388), which spans ~1 m at its base. Halley class buff-colored platy bedrock is present at the bottom of the scene (above the rover hardware). **(B)** An example of opaline silica sinter deposited in an active discharge channel of a hot spring at Tuja, Chile with similar characteristics. Scene spans ~1 m at its base.

Many of the individual silica nodules have millimeter-scale protuberances described as digitate protrusions or digitate structures (Fig. 3), which may have resulted from aeolian erosion (Ruff *et al.*, 2011), although their resemblance to hot spring microbial stromatolites on the Earth has been noted (Ruff and Farmer, 2016). The nodules have varied textures as observed on both disturbed and undisturbed surfaces. Where the rover wheel was used intentionally to expose fresh surfaces, two different disturbed nodules displayed porous, clastic textures, one with possible coated grains, the other with a brecciated appearance. Undisturbed nodules also display porosity, but in one case it is a distinctive sponge-like, vaguely honeycomb texture seemingly unaffected by aeolian erosion (Ruff *et al.*, 2011), which contrasts with the obviously smoothed porosity in other examples (Section 4).

Among the scattered outcrops of nodular silica is one occurrence of light-toned opaline silica regolith (soil), dubbed Gertrude Weise. This was inadvertently exposed by dragging of the rover's one inoperative wheel through otherwise dusty, dark-toned basaltic soil. The opaline silica soil is notably heterogeneous in particle size, with poorly sorted, very angular to sub-rounded particles ranging from cm-scale down to the limits of resolution of the Microscopic Imager (MI; ~30 μm/pixel), although the sand-sized fraction is dominant. The poor sorting, range of grain roundness, and paucity of fines indicate an immature soil that could have been produced by the action of the dragging wheel across silica-rich rock(s) rather than by natural soil-forming processes (Ruff *et al.*, 2011).

The silica soil provided the highest measured value of silica (91 wt % SiO_2) from Spirit's Alpha Particle X-ray Spectrometer (APXS) compared with all other measured high-silica materials, despite having a minor amount of basaltic soil contamination. The nodular silica outcrops invariably had much greater contamination from basaltic soil and airfall dust, contributing to the lower measured SiO_2 values (62–73 wt %) (Squyres *et al.*, 2008). After subtraction of a basaltic component, the nodular silica SiO_2 values reach 86 wt % (Ruff *et al.*, 2011). The greater abundance of Ti in the silica soil relative to the typical basaltic soil (~1.3 vs. ~0.75 wt % TiO_2) was suggested to represent passive enrichment, in concert with SiO_2 enrichment, due to acid-sulfate leaching (Squyres *et al.*, 2008). However, the nodular silica does not display the same trend, nor is there a sulfur enrichment in any of the opaline silica materials, weakening this hypothesis (Ruff *et al.*, 2011). Additionally, a recent reassessment of APXS measurements demonstrates that the Si/Ti ratio of the nodular silica rocks follows a dilution trend of Ti by the addition of silica rather than the fairly constant trend indicative of acidic leaching (Yen *et al.*, 2019).

The amorphous opal phase (opal-A) was identified in the outcrops and soil based on diagnostic features in thermal infrared (TIR) spectra from the Miniature Thermal Emission Spectrometer (Mini-TES; ~340–2000 cm^{-1}). An unusual feature near 1260 cm^{-1} in these spectra not typically found in opal-A was initially attributed to high emission angle viewing geometry (Ruff *et al.*, 2011). Subsequently, it was recognized as an attribute of halite-encrusted opal-A, consistent with silica sinter produced from alkali-chloride hot springs in a high-evaporation, low-precipitation environment (Ruff and Farmer, 2016). A distinctive spectral feature of the nodular silica also is evident at ~1 μm in visible/near-infrared observations from Spirit's multispectral Panoramic Camera (Pancam; ~0.4–1 μm) (Wang *et al.*, 2008).

Rice *et al.* (2010b) hypothesized that H_2O or OH associated with opaline silica was responsible for this feature, although dusty surfaces in some viewing conditions can mimic it. They developed an index for Pancam spectra known as the ''hydration signature,'' which is well correlated with high silica occurrences documented with Mini-TES and/or APXS.

3. Materials and Methods

3.1. Mars data

The Mars images and spectra included in this work were produced from the instruments shown in Table 1, which also includes sources for the data. Detailed descriptions of Spirit's payload are provided by Squyres *et al.* (2003) and references therein. Color Pancam images were produced according to methods described by Savransky and Bell (2004) and Bell *et al.* (2006). Images from Spirit's cameras are identified in figure captions by using a sol number (consecutive martian day since the beginning of the mission) and a sequence identifier of the form PXXXX where X is a numeral. Together, these two identifiers can be used to locate images from the websites listed in Table 1. Orbital images from the High-Resolution Imaging Science Experiment (McEwen *et al.*, 2007), Context Camera (Malin *et al.*, 2007), and Thermal Emission Imaging System Visible Imaging System (Christensen *et al.*, 2004) are identified in figure captions with the camera name and the alphanumeric sequence.

3.2. Earth field sites and samples

Interpretations of Mars images and compositional information benefit from terrestrial field sites that provide analogous characteristics. Here, we include observations and samples from hydrothermal settings in the United States and Chile. Samples from field sites were collected with permission where required.

3.2.1. Roosevelt Hot Springs and Opal Mound, Utah. These two sites, separated by ~4 km, are surface manifestations of the same active hydrothermal system driven by a young magmatic intrusion beneath the Mineral Mountain Range, northeast of Milford in southwestern Utah (Lynne *et al.*, 2005). Opal Mound is the largest sinter deposit evident at the surface and was emplaced from ~1900 to 1600 years ago from now-extinct hot spring vents on the Opal Mound fault (Lynne *et al.*, 2005). Smaller sinter deposits are present on the Hot Springs fault to the north and are part of the Roosevelt Hot Springs that were active until 1957 (Parry *et al.*, 1980). Currently, active surface manifestations are limited to fumaroles, steaming ground, and small seeps. Hot spring fluids were alkali-chloride in nature with a near neutral pH toward the end of their activity in the 1950s (Capuano and Cole, 1982).

3.2.2. El Tatio geyser field, Chile. This is the third largest hot spring/geyser field on the Earth, and at ~4300 m elevation, is one of the highest. It is located in the Altiplano of northern Chile, ~90 km north of San Pedro de Atacama. This location is noteworthy for its high evaporation and low precipitation rates, high solar ultraviolet flux, and diurnal freeze-thaw conditions (Nicolau *et al.*, 2014), which provide more Mars-like conditions than most hydrothermal settings on the Earth (Ruff and Farmer, 2016). More than 100 geysers and other manifestations, including flowing hot springs, hot pools, mud pots, and fumaroles, have been documented, spanning an area of ~10 km^2 (Glennon and Pfaff, 2003). Discharging waters are of alkali-chloride composition at near neutral pH (Nicolau *et al.*, 2014). Sinter deposits are abundant and include nodular forms with biomediated digitate structures (stromatolites) (e.g., Jones and Renaut, 1997; Barbieri *et al.*, 2014; Ruff and Farmer, 2016).

3.2.3. Puchuldiza-Tuja hydrothermal system, Chile. Similar to El Tatio, these two hydrothermal fields are part of the

Table 1. Data Sets Used in This Work and Their Sources

Instrument	*Description*	*Data source*
Spirit instruments		
Pancam: Panoramic Camera	13 Filter mast-mounted stereo imager spanning ~0.4 to 1.0 μm	Approximate true color, false color, anaglyph stereo, and named color panoramas (*e.g.*, McMurdo pan) are available at http://pancam.sese.asu.edu/images.html
MI: Microscopic Imager	Monochromatic arm-mounted high-resolution imager (~30 μm/pixel)	Single-frame and multi-frame mosaics are available at http://an.rsl.wustl.edu/mer
Navcam: Navigation Camera	Monochromatic mast-mounted stereo imager	Single-frame and multi-frame mosaics are available at http://an.rsl.wustl.edu/mer
Mini-TES: Miniature Thermal Emission Spectrometer	FTIR point spectrometer spanning ~5 to 29 μm (~2000 to 340 cm^{-1})	Mirror-dust corrected emissivity spectra are available at http://an.rsl.wustl.edu/mer
Orbiter instruments		
HiRISE: High-Resolution Imaging Science Experiment	High-resolution camera (~30 cm/pixel) on the MRO with 3 color filters centered on 536, 694, and 874 nm	https://hirise.lpl.arizona.edu
CTX: Context Camera	High-resolution (~6 m/pixel) monochromatic camera on MRO	http://global-data.mars.asu.edu/bin/ctx.pl

FTIR, Fourier transform infrared; MRO, Mars Reconnaissance Orbiter.

Central Andean Volcanic Zone and occur at high elevation (4100–4200 m) in the Altiplano. Both are adjacent to the active Isluga volcano and display hot springs and geysers among the various manifestations. Puchuldiza spans $\sim$1 km^2 and Tuja, located $\sim$6 km northwest, spans $\sim$0.15 km^2 (Tassi *et al.*, 2010). More than 100 active manifestations are present at Puchuldiza, with most having near neutral pH waters of alkali-chloride composition and abundant sinter deposits, some with nodular forms (Sanchez-Yanez *et al.*, 2017). Discharging waters at Tuja also are alkali-chloride, with pH spanning $\sim$5–6.5, although an extreme value of 1.76 has been documented (Tassi *et al.*, 2010). Abundant sinter deposits are present, and they include both nodular and digitate forms as presented in Section 4.

3.3. Laboratory studies

3.3.1. Spectroscopy. TIR spectra were acquired from selected field samples to characterize their mineralogy and allow for comparisons with Mini-TES spectra. A laboratory spectrometer (Nicolet iS50R; $\sim$200–2000 cm^{-1}) with a custom apparatus for emission measurements was used. Data were measured and calibrated to emissivity according to the technique presented by Ruff *et al.* (1997). Hand samples were measured on unprepared surfaces after heating in an oven for at least 2 h at 80°C to drive off adsorbed water and to enhance the emission measurement.

3.3.2. Sandblasting. In an effort to investigate the role of aeolian abrasion in shaping the morphology and texture of the Home Plate opaline silica deposits, we have sandblasted samples in a cabinet containing basaltic sand driven by compressed air. Sand particle size was $\sim$250 μm (crushed and sieved particles from Amboy Crater basalt), which is the median size range of sand particles observed by Spirit in the ''El Dorado'' ripple field (Sullivan *et al.*, 2008). Airflow was controlled to drive sand at a rate of $\sim$20 m/s, which is at the low (conservative) end of the range (20–40 m/s) of wind speeds estimated to have caused the observed migration of sand ripples while Spirit was adjacent to Home Plate (Sullivan *et al.*, 2008). Although this was an unusually strong wind event, such relatively rare events are assumed to have the most influence on the landscape (Sullivan *et al.*, 2008). For the purposes of our laboratory-based effort, we used this airflow velocity to compress in time a process of erosion that on Mars may have occurred over millions or perhaps billions of years. The direction of the airflow was varied over the course of a run, spanning impact angles of roughly 20–80° (90° is normal incidence) across an azimuth range approaching 180°. This approach perhaps better addresses the uncertainty of the direction of winds over time as well as the multidirectional impact angles that presumably arise from passing dust devils (thermal vortices), which are well documented in Gusev crater (e.g., Sullivan *et al.*, 2008). The duration of a given run spanned $\sim$5–20 min depending on the susceptibility to abrasion of a given sample, as described in Section 4.

The sandblasting was performed at ambient atmospheric pressure and temperature, despite the known low pressure of the current martian atmosphere (600 Pa average). Although temperature is not a factor, atmospheric pressure (density) is a factor in the particle flux variable, q, of the abrasion rate relationship

$$R = qfS_a \quad (1)$$

where f is the wind frequency, and S_a is the susceptibility to abrasion (Greeley *et al.*, 1982). However, our aim is not to quantitatively address abrasion rate, as was done for coated rocks at the Mars Pathfinder site by Kraft and Greeley (2000). Rather, it is to demonstrate the kind of changes in morphology and texture of opaline silica materials that could arise from prolonged exposure to wind-blown sand on Mars. In this context, the rate of abrasion, and hence the atmospheric pressure, is not a concern.

4. Results

Previous hypotheses for the origin of opaline silica at Home Plate generally include two processes involving hydrothermal activity, namely, fumarolic acid-sulfate leaching and precipitation from spring-related hydrothermal fluids. The proximity of S-rich soils has been used to bolster the case for the former, despite the recognition that both processes can occur within the same hydrothermal system (Squyres *et al.*, 2008; Wang *et al.*, 2008; Yen *et al.*, 2008). Although the S-rich soils and opaline silica deposits are not necessarily related (Yen *et al.*, 2008), Section 4.1 documents examples of hydrothermal environments where both are present. Section 4.2 expands on previous efforts to relate the morphology and textures of the Home Plate silica deposits to formation process(es) by using new field observations and laboratory efforts. Section 4.3 incorporates new and existing observations from Home Plate pertaining to the stratigraphy of the silica deposits, with comparisons to terrestrial silica producing environments. Finally, in Section 4.4, we provide new observations that support the possibility of a hot spring vent mound adjacent to Home Plate.

4.1. Proximity to S-rich soils

There are abundant examples of the co-occurrence of fumarolic and hot spring activity on the Earth that include elemental S and S-rich minerals in rocks and soils in close proximity to hot spring sinter deposits (e.g., Day and Allen, 1925; White, 1957; Ellis and Mahon, 1964; Sorey *et al.*, 1991; Bignall and Browne, 1994; McHenry *et al.*, 2017). In fact, the co-occurrence of acid-sulfate leaching and hot spring sinter deposits is a recognized feature of hydrothermal systems throughout the geological record used to guide mineral exploration (e.g., Tritlla *et al.*, 2004; Van Kranendonk and Pirajno, 2004; Bethke *et al.*, 2005; Sillitoe and Hedenquist, 2005). Roosevelt Hot Springs is an example of such a co-occurrence. In this case, the hydrothermal system is currently transitioning from hot spring to fumarolic activity during a waning phase of surface activity. A common late-stage process in the evolution of hydrothermal systems is phase separation due to subsurface boiling, which can lead to the escape of gaseous hydrogen sulfide that combines with surface water to form sulfuric acid (e.g., White, 1957; Truesdell *et al.*, 1977; Shinohara *et al.*, 1993). The low pH fumarolic gases alter the host materials, producing an overprint of acid sulfate alteration. Such overprinting may have occurred within the Home Plate hydrothermal system, a scenario that

has not been previously proposed but is widely recognized on the Earth (e.g., Bignall and Browne, 1994; Lynne and Campbell, 2004; Van Kranendonk and Pirajno, 2004; Van Kranendonk, 2006; Lynne *et al.*, 2007; Campbell *et al.*, 2019).

The transition to fumarolic activity at Roosevelt Hot Springs is best seen on a fault-bound hill slope where active acid-sulfate leaching has thoroughly altered the granitic regolith. A ragged margin is evident that divides the pervasive alteration below from the upper, patchy occurrences of sinter from now extinct hot springs, reflecting a declining water table (Fig. 4). Steaming fumaroles emitting H_2S gas and minor warm seeps with mildly acidic (pH 5–6) thermal waters (50–60°C) are present in the altered zone. Samples were not obtained from this zone, but Parry *et al.* (1980) reported that the overlying alluvium has been partially to totally altered to alunite ($KAl_3(SO_4)_2(OH)_6$) and opal, with hematite staining the opal and filling small intergranular pores. The hematite includes pseudomorphs after pyrite within opal cement. The alunite derives from alteration of the granitic regolith that dominates the alluvium.

At the top of this hill is an extinct hot spring pool, evident from a sinter deposit partially encircling a zone of sinter regolith and other detrital materials (Fig. 5). When overturned to a few centimeters, the regolith/soil displays elemental sulfur along with the odor of H_2S and a temperature of $\sim$50°C. These features likely reflect acid-sulfate steam reaching the surface through the same plumbing system that fed the original hot spring, an indication of fumarolic overprinting of the original sinter deposit.

4.2. Morphology and texture

The morphology (shape) and texture (surface or interior details) of the Home Plate opaline silica rocks reflect the processes that formed and modified them. Ruff *et al.* (2011) interpreted the nodular morphology as the result of erosion, although the possibility that it is, in part, a primary characteristic also was suggested. Likewise, the digitate structures were assumed to be the result of aeolian abrasion. Subsequently, however, the similarity of these features to those displayed by sinter deposits within hot spring and geyser discharge channels at El Tatio was recognized (Ruff and Farmer, 2016). In addition, opaline silica nodules of comparable size and morphology, and with halite encrustations, also have been found to be common features of discharge channels at Puchuldiza and Tuja (Fig. 6). Similar to El Tatio, nodular silica is found in the mid- to low-temperature (<40°) portions of these channels. We note that the digitate structures tend to be more prominent at Tuja compared with the bumpy expression typical of Puchuldiza nodules (Fig. 6).

At El Tatio, some digitate structures were shown to be biomediated stromatolites (Ruff and Farmer, 2016). An example of a digitate silica nodule from Tuja also displays fine, stromatolite-like internal laminations on a surface exposed after it was chiseled from the lithified channel floor on which it was anchored (Fig. 6). We have found anchored nodular silica among discharge channels at El Tatio and Puchuldiza as well, which presumably reflects the depositional accretion process. However, nodules with no point of attachment also are common. Anchored silica nodules are evident at Home Plate in multiple locations where they were rolled over by the rover wheels without being disturbed (Ruff *et al.*, 2011).

Although a primary origin is possible for the digitate structures among the Home Plate area opaline silica nodules, they surely would have been subjected to some degree of aeolian abrasion since their formation. This motivates the question of how they might have been reshaped over time and exposure to wind-blown sand. We have approached

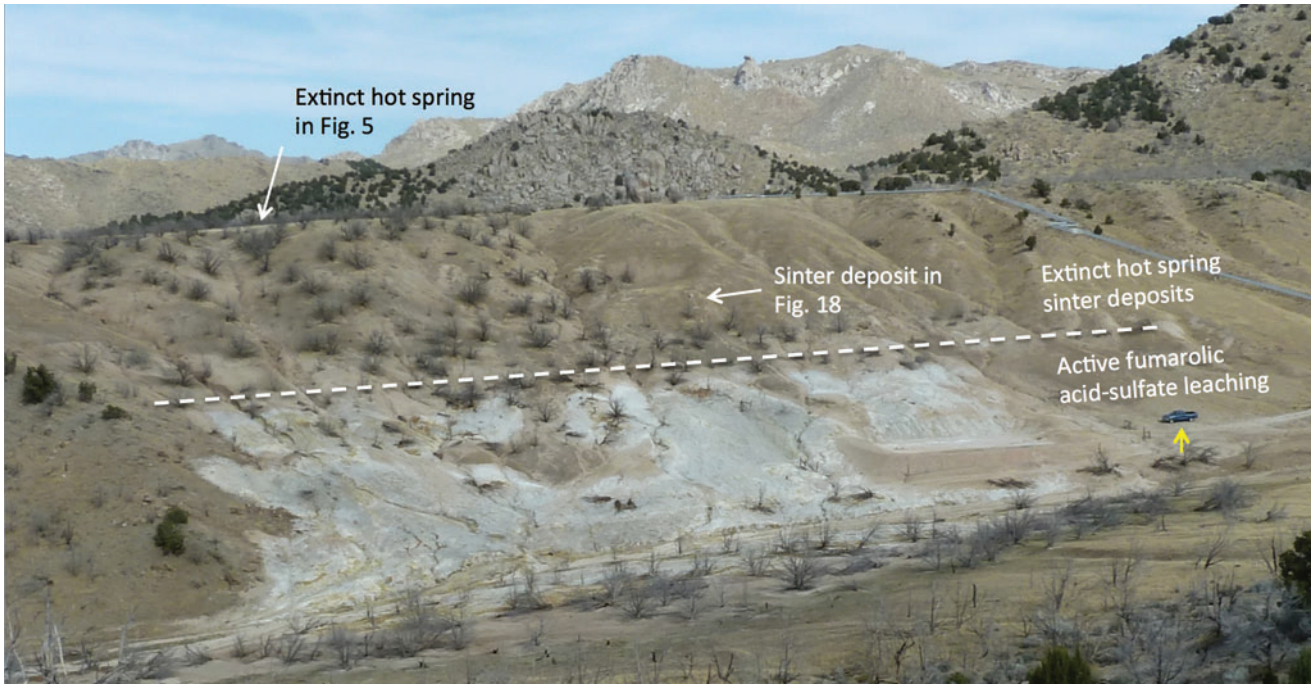

FIG. 4. Features of hydrothermal activity at Roosevelt Hot Springs, Utah. Former hot springs deposited sinter around pools and within discharge channels in the upper portion of the scene. Now only fumarolic activity remains, producing intense alteration in the lower portion. Yellow arrow points to vehicle for scale.

FIG. 5. A former Roosevelt Hot Springs pool displays silica sinter at the rim and S-rich soil from active fumarolic processes in the interior. Rectangle represents the inset view showing elemental S coating soil clods.

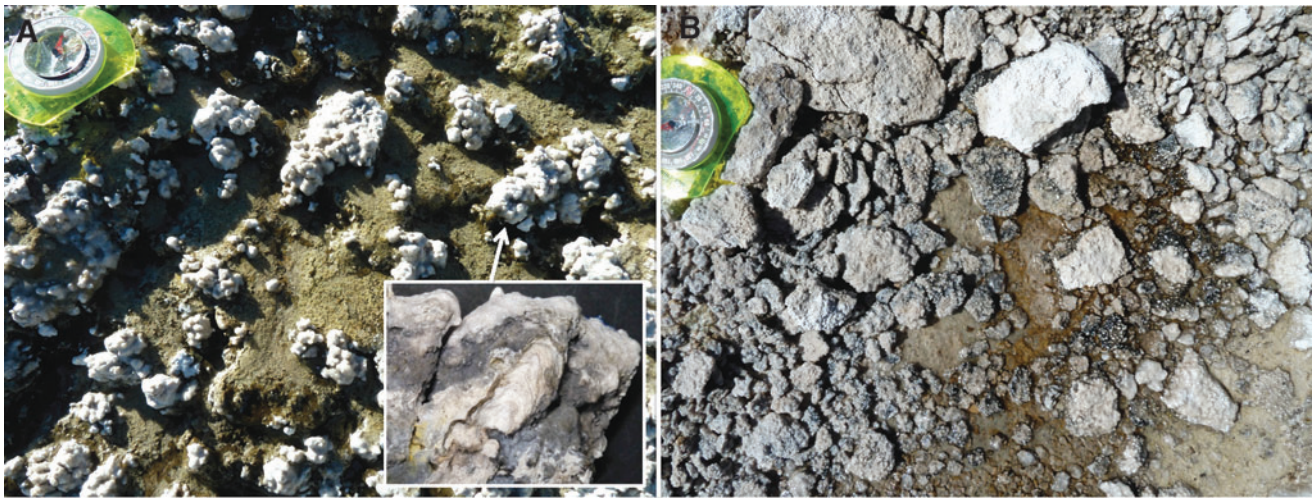

FIG. 6. Sinter deposits in hot spring discharge channels at **(A)** Tuja, Chile and **(B)** Puchuldiza, Chile. Both include nodular morphology with digitate structures, although the latter are more prominent in the Tuja example. The inset in **(A)** shows a layered stromatolite-like feature exposed on the underside of the indicated nodule after it was chiseled from the channel floor.

this question by sandblasting two field samples with different characteristics. One is the piece of digitate, nodular silica from Tuja described above and shown in Fig. 6, which represents fresh sinter from an active discharge channel. The other comes from one of the extinct Roosevelt Hot Springs that has been exposed to surface weathering for >60 years (hot spring activity ended there in 1957; Capuano and Cole, 1982). The Tuja sample was quickly eroded with only 5 min of sandblasting, essentially destroying the digitate structures while revealing internal laminations within the basal parts of the eroded digitate structures. In contrast, the initially stubby structures on the Roosevelt sample became more accentuated after ~20 min of sandblasting (Fig. 7). This contrast in the effects of erosion reflects the relative hardness of fresh (softer) versus aged (harder) sinter.

Herdianita *et al.* (2000) demonstrated that aging of sinter is accompanied by dehydration, loss of porosity, and an increase in density, which translates to an increase in hardness over time. Soft and friable fresh sinter becomes harder with age after cessation of hydrothermal circulation, even while retaining its opal-A mineralogy (Herdianita *et al.*, 2000). Lynne and Campbell (2004) developed a friability index for opaline silica sinter and indicated that porous friable sinter is a product of polymeric silica deposition, whereas indurated opaline sinter forms during monomeric deposition. Laboratory TIR spectra of the fresh Tuja sinter and aged Roosevelt Hot Springs sinter reveal opal-A mineralogy for both materials, despite the obvious difference in hardness.

Another consideration for Home Plate nodular silica is whether aeolian abrasion can form digitate structures where none was initially present. For example, there are many forms of sinter, both nodular and otherwise, that do not display digitate structures but perhaps would through aeolian abrasion. To test this scenario, we selected a sample of sinter breccia from El Tatio for sandblasting. Sinter breccia is composed of fragments of earlier generations of sinter that are deposited and cemented by opaline silica to form new rock, which is common in hot spring environments (e.g., Campbell *et al.*, 2001; Jones and Renaut, 2003; Hinman and Walter, 2005; Hamilton *et al.*, 2018). Because of the fragmental nature of sinter breccia, it commonly contains clasts of varying hardness that might allow for preferential erosion that could lead to digitate or protruding structures. Given that some of the Home Plate silica rocks appear to have a breccia texture consistent with sinter breccia (Ruff *et al.*, 2011), the use of such material was especially appropriate for a sandblasting experiment.

We subjected a sinter breccia sample from El Tatio to ~15 min of sandblasting, which produced no protrusions. Instead, the porous nature of the breccia was enhanced, clasts were smoothed and rounded, and dimpled surfaces emerged, resulting in a texture that resembles the unusual texture of ''Nancy Warren,'' one of the Home Plate silica

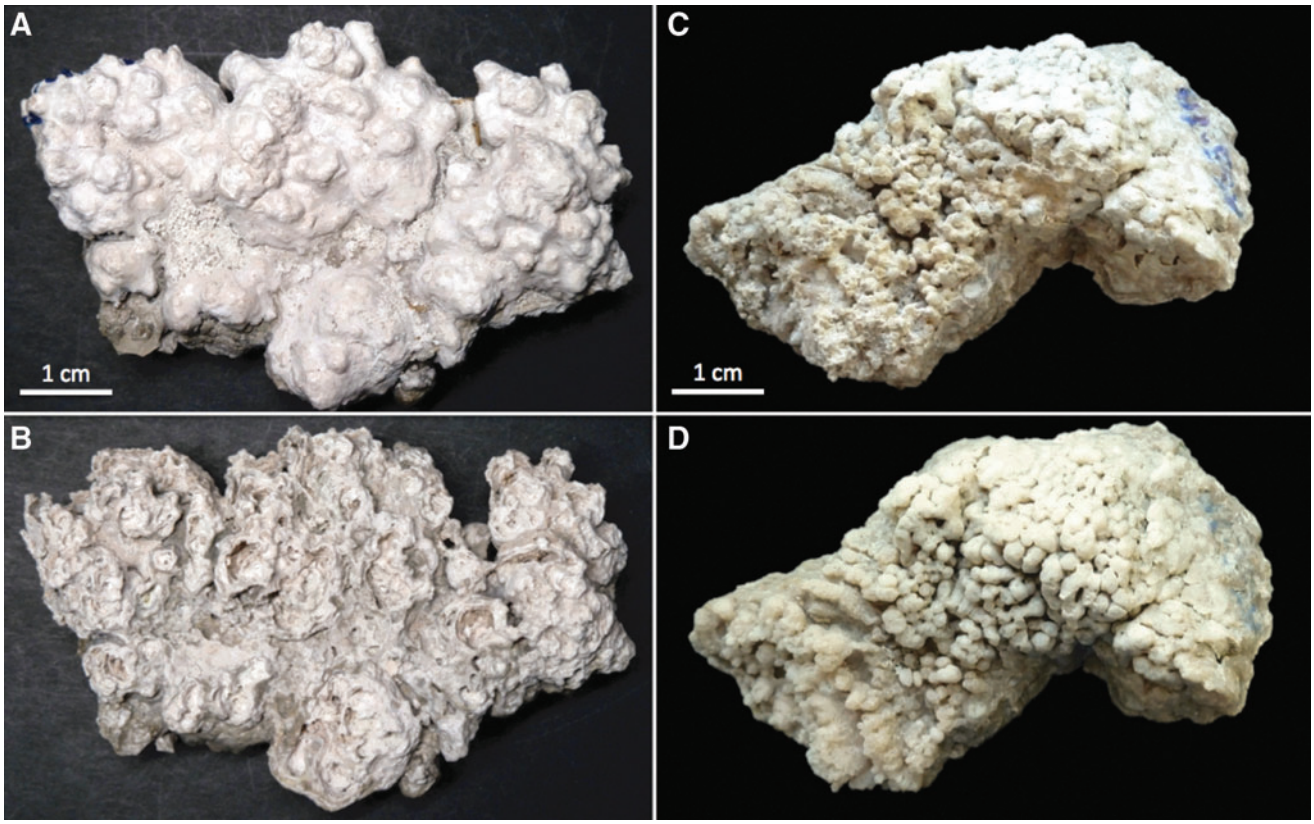

FIG. 7. Nodular silica sinter before and after sandblasting. **(A)** A fresh sample from the hot spring discharge channel at Tuja, Chile (Fig. 6) displays prominent digitate structures, which are severely eroded after sandblasting **(B)**. **(C)** An aged sample from an extinct hot spring at Roosevelt Hot Springs, Utah displays stubby digitate structures, which become accentuated after sandblasting **(D)**.

rocks observed with the MI (Fig. 8). Tabular clasts are evident in both the sandblasted El Tatio sample and Nancy Warren, which in sinter breccia is a reflection of its fragmental origin. The proximity of Nancy Warren to the best example of breccia texture around Home Plate, which occurs in the disturbed rock dubbed Norma Luker about 1 m away, strengthens the case that its unusual texture represents naturally sand-abraded breccia.

Another unusual texture observed with the MI among the opaline silica rocks around Home Plate is a sponge-like surface on the nodular rock with prominent digitate structures dubbed Elizabeth Mahon (Fig. 9A; Ruff *et al.*, 2011). Ruff and Farmer (2016) presented a possible analogous texture observed on a sinter sample from El Tatio. We now recognize a more compelling analogue from the Roosevelt Hot Springs example described above in which late-stage fumarolic activity is present within a soil-filled extinct hot spring (Fig. 5). The sinter deposit at the rim of the former hot spring pool has a remarkably similar sponge-like or honeycomb texture (Fig. 9B) that is atypical of primary sinter texture. It likely arises through corrosion from fumarolic activity, a scenario outlined by Rodgers *et al.* (2004) for long-lived hydrothermal fields where changing hydrologic conditions cause steam condensate to permeate older sinter, leading to silica dissolution, remobilization, and reprecipitation.

4.3. Stratigraphy

The stratigraphic relationship of the nodular opaline silica outcrops with other rock units adjacent to Home Plate remains unresolved. Squyres *et al.* (2008) first noted that the nodular silica outcrops cover the Halley class buff-colored platy outcrops in multiple places on the east side of Home Plate (Fig. 10). This constitutes a stratiform relationship between older Halley rocks and younger silica rocks as noted by Ruff *et al.* (2011). Although underlying contacts are obscured by regolith in some places, nowhere are the opaline silica deposits observed to lie on a different lithologic unit, nor has any direct overlying contact been observed. These observations lead to two possible stratigraphic models (Fig. 11). In model 1, the opaline silica deposits are

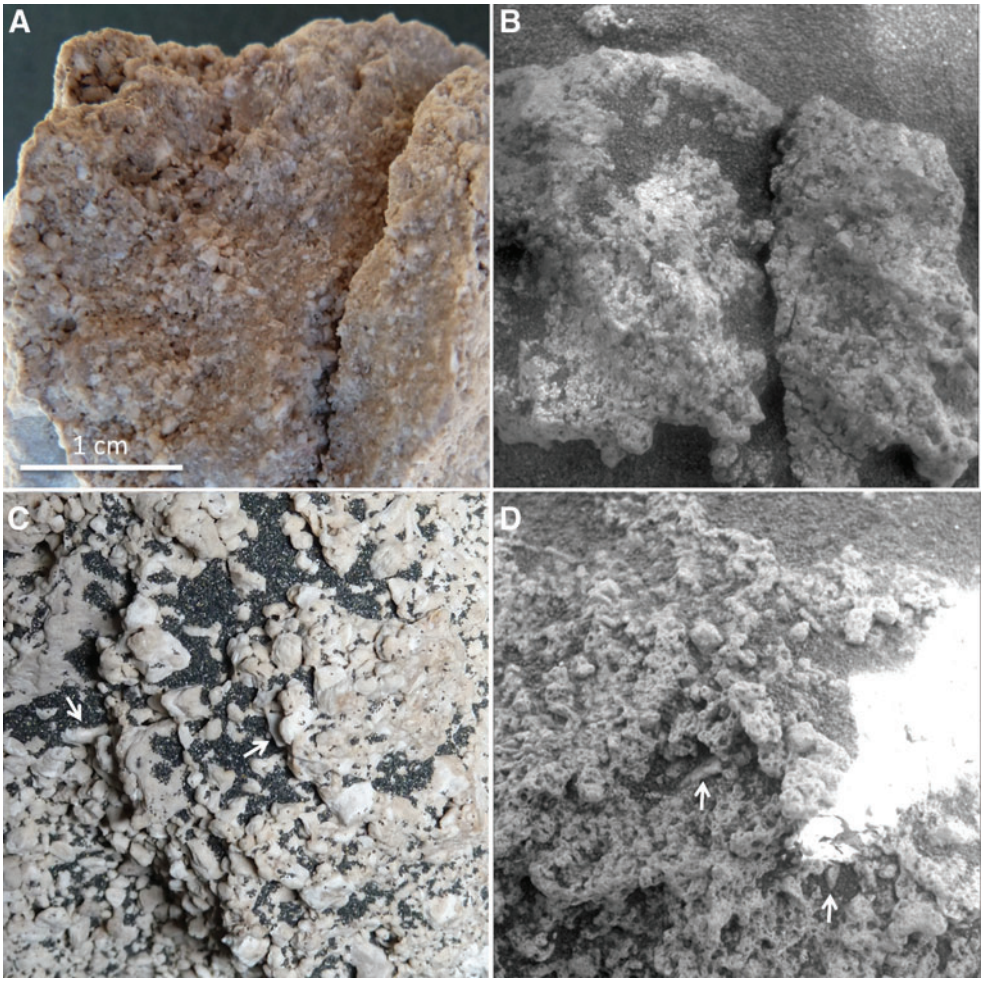

FIG. 8. Breccia texture in sinters from El Tatio and comparable texture in Home Plate silica rocks. **(A)** A fresh surface of El Tatio sinter breccia shows porosity and clasts that resemble those from **(B)** ''Norma Luker,'' a silica rock broken open or overturned by the rover's wheel (MI image, sol 1291, P2956). **(C)** The sandblasted and basalt sand-covered surface of another El Tatio sinter breccia resembles **(D)** ''Nancy Warren,'' a silica rock exposed to aeolian abrasion <1 m from Norma Luker (MI image, sol 1227, P2976). Arrows in **(C)** and **(D)** highlight similar emergent tabular clasts. Sunlight appears saturated in a portion of this otherwise shadowed scene. All images are at the same scale. MI, Microscopic Imager.

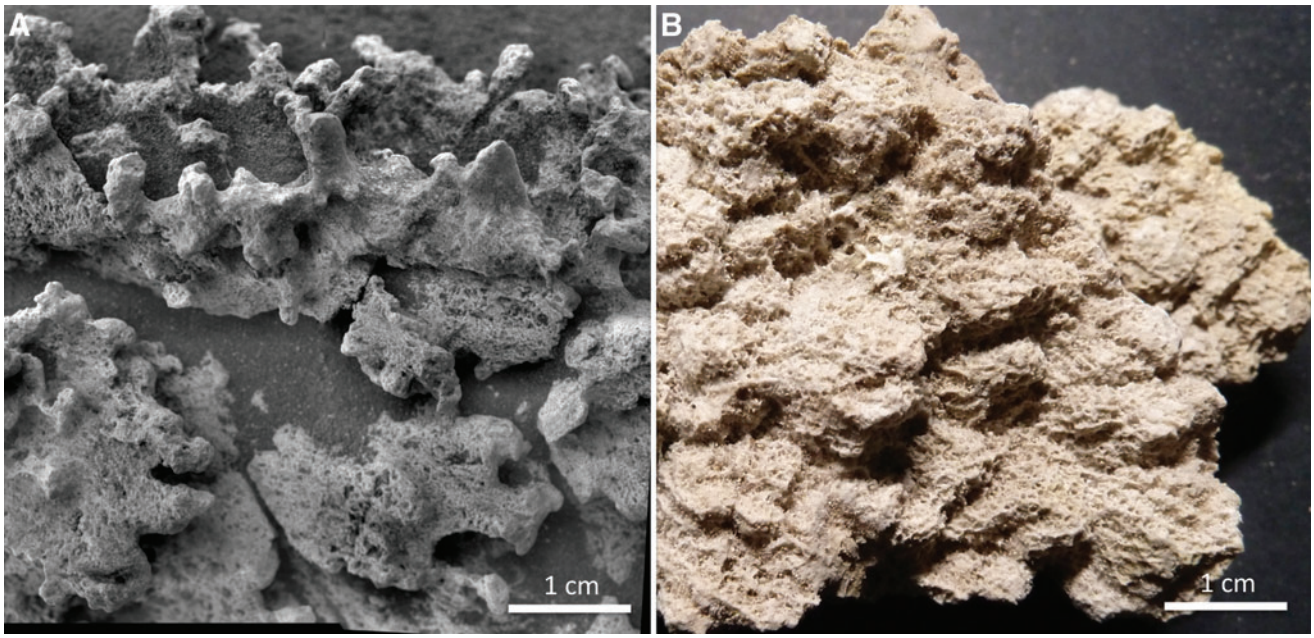

FIG. 9. Unusual sponge-like texture on silica rocks. **(A)** Elizabeth Mahon has prominent digitate structures that appear smooth compared with sponge-like texture of the lower portions (MI mosaic, sol 1157, P2976). **(B)** A piece of sinter from the rim of the extinct Roosevelt Hot Spring shown in Fig. 5 has a remarkably similar texture, likely due to corrosion from late-stage fumarolic activity.

part of the ancient stratigraphy of the Home Plate area, forming a discontinuous layer deposited above the Halley class unit and below the volcaniclastic and basaltic units. The buried Halley class rocks and opaline silica deposits were then exhumed by erosion of the overlying units. In model 2, the opaline silica deposits are younger (no age constraints) than all of the Home Plate volcanic units, deposited on re-exposed Halley class after a period of erosion of the overlying units.

The lack of overlying contacts seems to favor model 2, yet there are at least two locations that suggest that the opaline silica deposits were buried by the volcaniclastic and

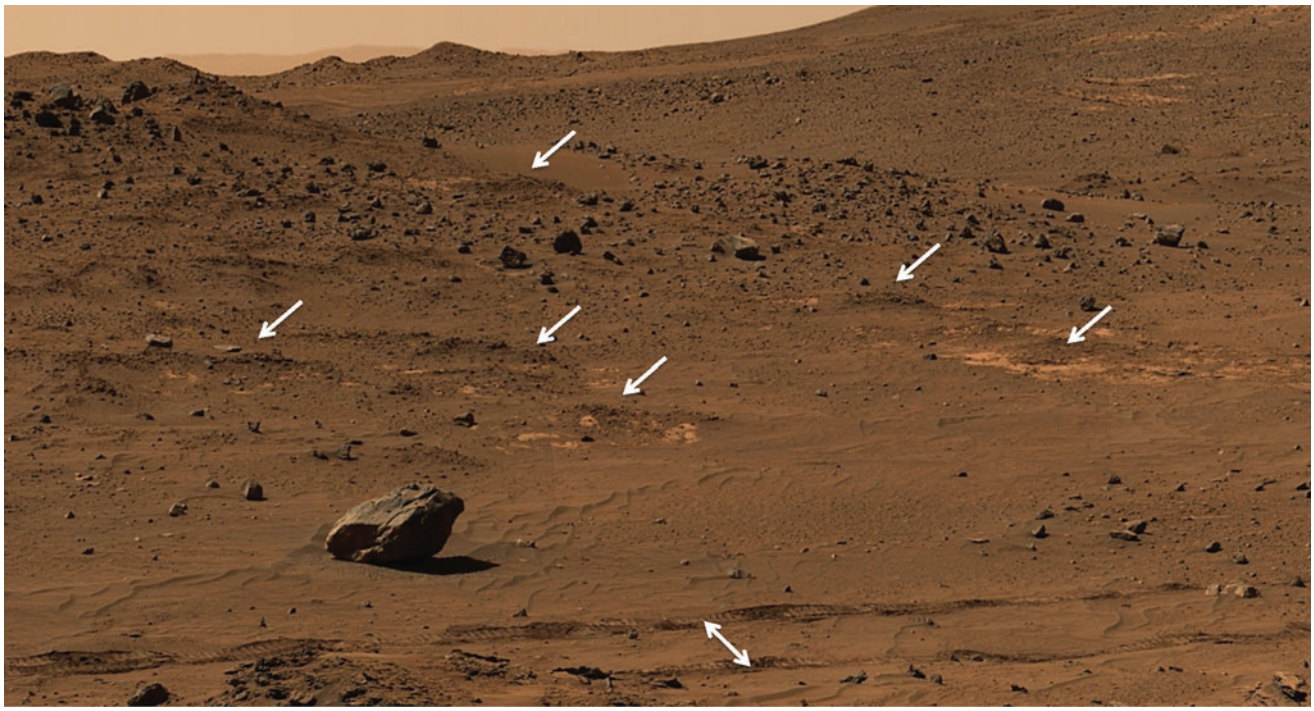

FIG. 10. Discontinuous nodular silica outcrops displaying stratiform nature and sharp contact relationship with underlying buff-colored platy bedrock. Arrows point to examples in this cropped portion of the Pancam ATC McMurdo panorama looking NE from Low Ridge. Rover wheel tracks indicated by the double-headed arrow are $\sim$1 m apart.

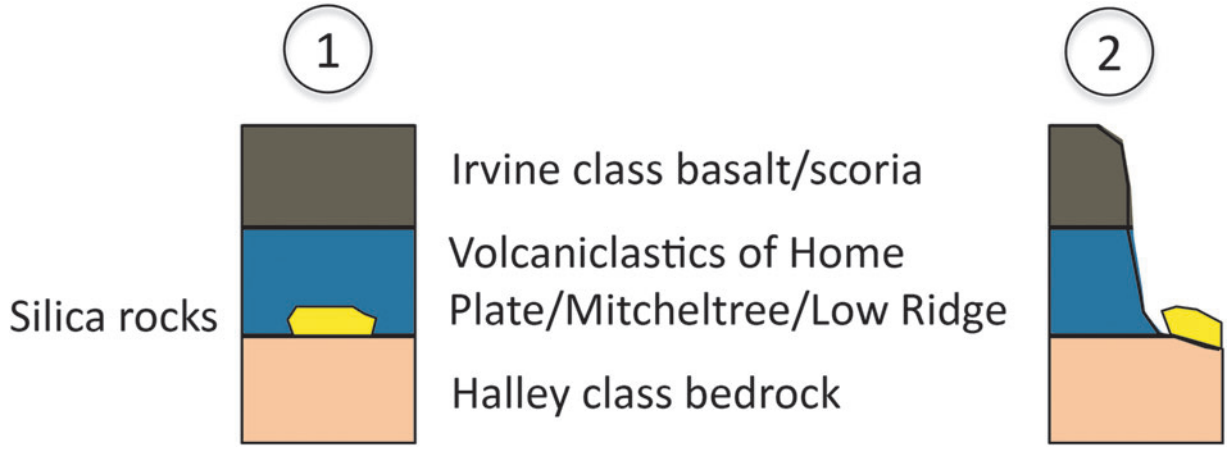

FIG. 11. Conceptual stratigraphic models for Home Plate and rocks to the east. In model 1, silica rocks (in yellow) are emplaced on the Halley unit followed by volcaniclastics and basalt/scoria. Subsequent erosion re-exposes the silica rocks and Halley unit. In model 2, silica rocks are emplaced on the Halley unit after emplacement and erosion of the other units. The vertical section represents ~2 m, but units are not shown to scale.

basaltic rocks. In the Eastern Valley, an outcrop known as Clara Zaph contains nodular opaline silica <2.5 m from Home Plate volcaniclastic rocks that dip away from it (Fig. 12). Although there is no definitive contact relationship exposed in this location, it appears that the nodular silica outcrop is being exhumed from a pebbly basal unit of Home Plate deposits. This suggests that the opaline silica outcrop predates Home Plate volcaniclastic rocks.

Another example of a possible overlying contact relationship occurs among outcrops at the southern tip of Mitcheltree Ridge, a long topographic feature parallel to the eastern margin of Home Plate (Fig. 2) that hosts volcaniclastic and basaltic rocks comparable to those of Low Ridge (Arvidson *et al.*, 2008). Here, a small buff-colored platy outcrop with characteristics consistent with the recognized stratigraphy of Halley class rocks lies at the base of the ridge (Fig. 13A). Nodular rocks, one with prominent digitate structures, are present on top (Fig. 13B). Although no Mini-TES spectra were acquired here, the Pancam hydration signature (Fig. 13C) highlights portions of the nodular rocks with the same intensity as observed on targets shown by Mini-TES elsewhere to have opaline silica. It is noteworthy that some

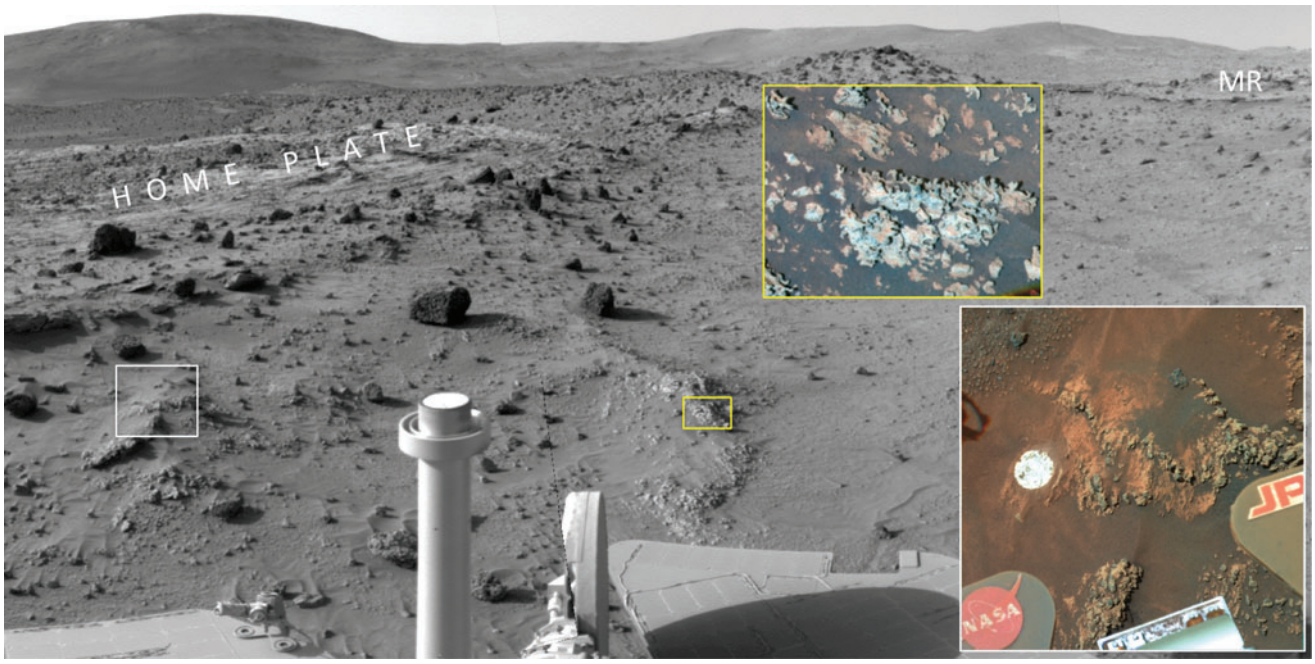

FIG. 12. Stratigraphy at the eastern edge of Home Plate. The cropped Navcam mosaic (sol 1121, P0615) includes a portion of Mitcheltree Ridge (MR) to the right. Yellow rectangle represents the position of the yellow-lined inset false-color view of Elizabeth Mahon (sol 1160, P2582 spanning ~15 cm), part of Clara Zaph, the closest nodular digitate silica outcrop to Home Plate. White rectangle represents white-lined inset false-color view (sol 1180, P2596 spanning ~35 cm) of cemented pebbly volcaniclastic rocks that are basal to the Home Plate rocks, from which the nodular silica appears to be emerging. White spot is specular glint from the ~4 cm diameter circular area brushed with the Rock Abrasion Tool.

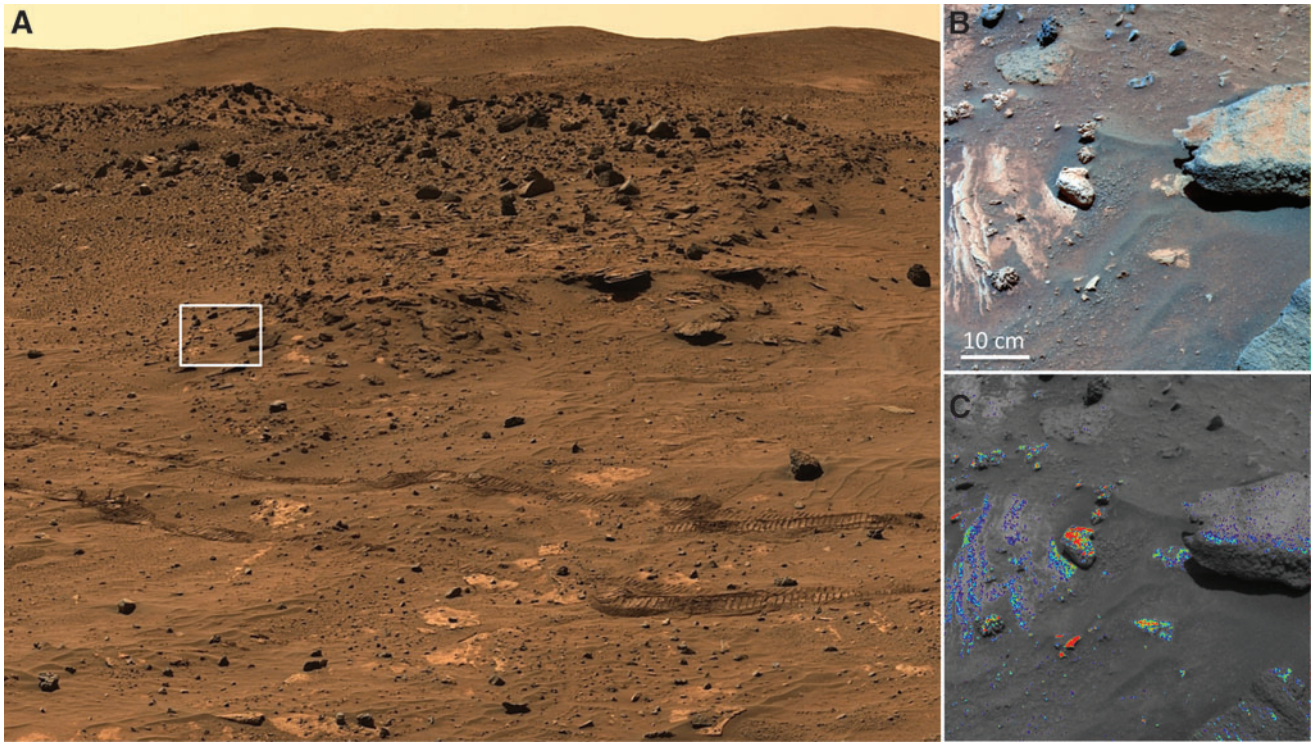

FIG. 13. Evidence for nodular opaline silica in contact with Halley class rocks at the southern tip of Mitcheltree Ridge. **(A)** Cropped portion of the Pancam ATC McMurdo panorama looking N from Low Ridge showing context of Halley class buff-colored platy bedrock. Rectangle represents view in **(B)** and **(C)**. Rover tracks are ~1 m apart. **(B)** A false-color Pancam image (sol 1113, P2456) of unnamed rocks includes light-toned nodular rocks, one with pronounced digitate structures, appearing to erode from the layered Halley class outcrop. Bluish rocks include spherical grains, presumably accretionary lapilli similar to those in volcaniclastic rocks at Low Ridge. **(C)** The Pancam hydration signature supports an opaline silica composition for the nodular rocks and possible silicification of Halley rocks. Blue to red hues show low to high values, respectively, with red corresponding to the value observed for the known opaline silica materials at Gertrude Weise and Elizabeth Mahon.

of the intact surfaces and fragments of platy rocks have intense hydration signatures, likely too intense to be the false positives attributed to surface dust viewed at certain angles (Rice *et al.*, 2010b), as found on portions of some of the adjacent bluer rocks. Instead, these platy rocks may represent alteration of Halley rocks by silica-rich fluids (silicification) during the deposition of the likely nodular silica rocks, as discussed in Section 5.1.

The combination of color, morphology, and hydration signature makes a strong case that this location hosts nodular and digitate opaline silica in contact with underlying Halley class outcrop. The bluer rocks in this location, the largest of which display textures that include spherical grains interpreted as accretionary lapilli, are comparable to volcaniclastic rocks elsewhere on Mitcheltree and Low Ridge. These volcaniclastic rocks appear to overlie and thus appear to be younger than the apparent nodular opaline silica. If the opaline silica were younger here, the overlying volcaniclastic rocks likely would have been silicified as suggested above for the Halley rocks, but this is not the case.

Another location provides support for silicification of Halley class rocks in the Eastern Valley. Within ~1 m of the Gertrude Weise silica-rich soil deposit, Ruff *et al.* (2011) documented two Pancam and Mini-TES targets dubbed Ethyl Boyce and Joanne Weaver. Here, the Halley buff-colored platy rocks are exposed and directly overlain by nodular rocks. The platy rocks dominate the Mini-TES field of view (FOV) in each case, yet the spectra display evidence for opaline silica (Supplementary Fig. S1). The presence of opaline silica here also is indicated by the hydration signature from Pancam on the Ethyl Boyce target. Unfortunately, the Pancam observation of Joanne Weaver was limited to three of its 11 unique spectral filters, insufficient to investigate the hydration signature. Although not suggested by Ruff *et al.* (2011), spectral evidence for opaline silica among the Halley class rocks at this location may be an indication of their silicification.

Given that the nodular silica rocks have only been found in contact with the Halley class unit, and this unit displays evidence for silicification, two scenarios are most likely for the timing and mode of silica emplacement from hydrothermal activity. First is that silica was emplaced either as sinter deposits on exposed Halley class rocks or through acid-sulfate alteration of these rocks, followed sequentially by emplacement of the volcaniclastic units and then Irvine class rocks. The second scenario is that the silica was emplaced after the deposition and erosion of Halley class rocks and the overlying units, either as sinter deposits or through acid-sulfate alteration. In this scenario, only Halley class rocks were subjected to silica emplacement. As discussed in Section 5, however, the emplacement of silica as sinter deposits lying stratigraphically on top of Halley rocks is

the scenario that is the most consistent with the observations outlined above. This scenario is supported by evidence for a nearby hot spring vent mound described below.

4.4. Candidate hot spring vent mound

The final phase of the Spirit mission occurred at the base of the western scarp of Home Plate. From there, an unusual mound-shaped structure ~15 m across at its base and 1–2 m high was observed <50 m west of Home Plate (Fig. 2). Dubbed Pioneer Mound, it was viewed from multiple angles with Pancam and Mini-TES. Its rocks have a distinctive reddish hue and clustered distribution compared with the scattered bluish basaltic rocks that surround it (Fig. 14). Because these characteristics are found in all the known opaline silica outcrops around Home Plate, the rocks of

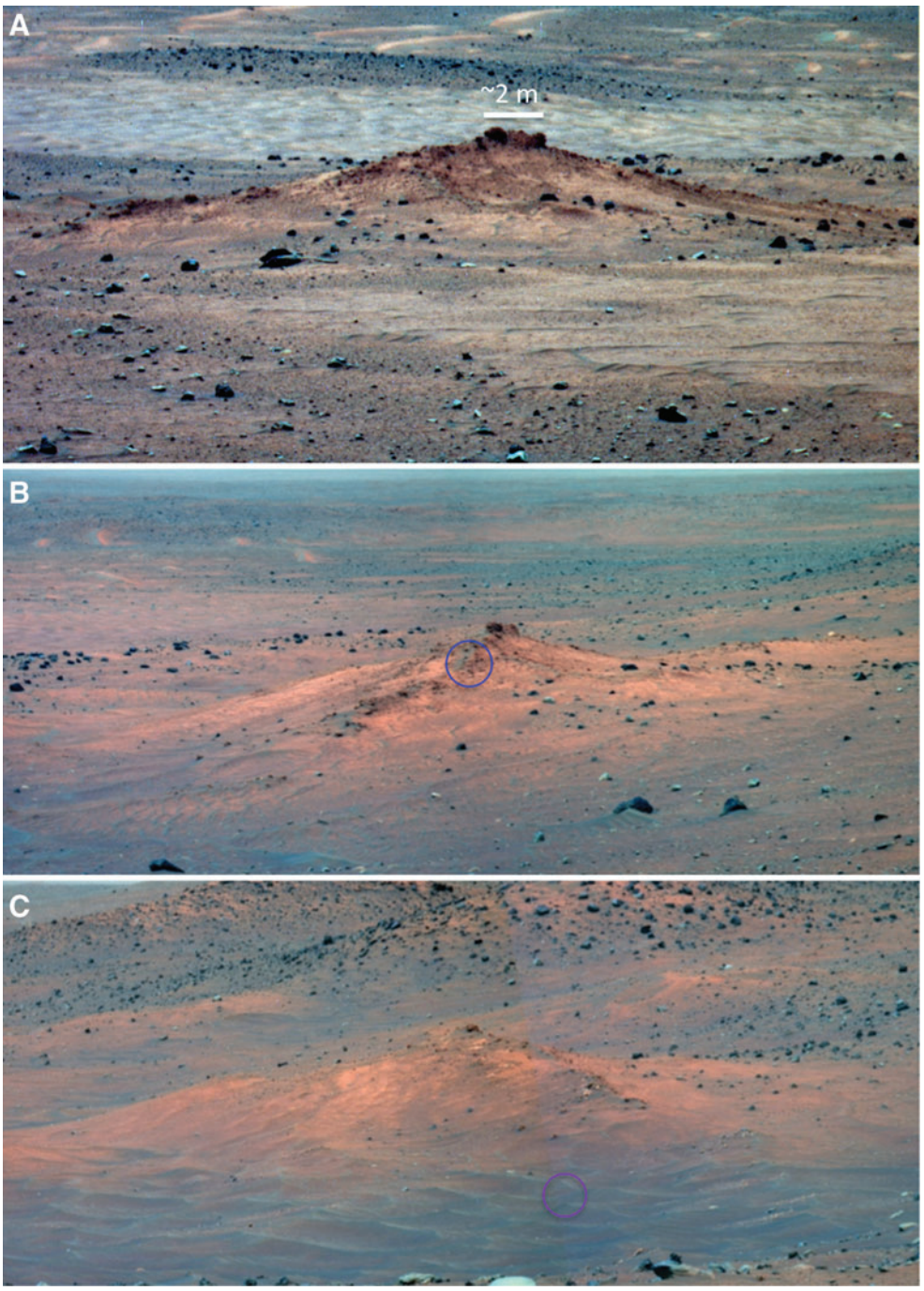

FIG. 14. Pioneer Mound, a possible hot spring vent mound, viewed from multiple positions in the West Valley of Home Plate. Clusters of reddish-hued rocks, distinct from the surrounding scattered rocks with bluish hues in these Pancam false-color images, are consistent with all known opaline silica outcrops. **(A)** Single frame acquired on sol 1860 (P2561). **(B)** Two-frame mosaic acquired on sol 1865 (P2553). Blue circle represents the Mini-TES FOV on a cluster of reddish-hued rocks for spectrum in Fig. 15. **(C)** Two-frame mosaic acquired on sol 1898 (P2377). Purple circle represents the Mini-TES FOV on aeolian bedforms for spectrum in Fig. 15. FOV, field of view; Mini-TES, Miniature Thermal Emission Spectrometer.

Pioneer Mound were suggested to be composed of opaline silica as well (Ruff *et al.*, 2011). The opaline silica composition of Pioneer Mound rocks remained speculative, because it is too distant for reliable Pancam hydration signature analysis (Rice *et al.*, 2010b) and it was observed at a time in the mission of extreme dust contamination of the Mini-TES optics. Now we have recognized a method for obtaining useable spectral information from the dust-encumbered Mini-TES spectra.

The exposed pointing mirror in the periscope-like mast used by Mini-TES was first contaminated by dust during aeolian activity on ~sol 420 (Ruff *et al.*, 2006). A robust correction was developed and applied successfully to Mini-TES spectra through sol 1220, after which dust from a planet-encircling dust event produced additional contamination that was no longer fully correctable (Ruff *et al.*, 2011). However, spectral features of a given target are still discernable, especially in the long wavelengths (low wavenumbers; $<600\,cm^{-1}$) of Mini-TES spectra, where dust has relatively weak features (Ruff *et al.*, 2006, 2011). With the benefit of Mini-TES spectra obtained from known opaline silica rocks before and after the sol 1220 mirror-dust build-up, we have compared these spectra with those of Pioneer Mound.

The best Mini-TES observation of Pioneer Mound occurred on sol 1864 from its closest vantage point (~35 m), providing viewing geometry that maximized the FOV on a cluster of reddish-hued rocks (Fig. 14B). Applying the standard mirror-dust correction (Ruff *et al.*, 2011) to the spectrum reduces but does not eliminate the spectral contributions of dust. The same correction was applied to Mini-TES spectra of the known opaline silica rock Nancy Warren acquired before and after the sol 1220 mirror-dust build-up (sol 1189 and 1223, respectively). A second rock called Stapledon was observed with Mini-TES only after the dust build-up (sol 1788), but it was recognized as another nodular silica rock based on color, morphology, and the APXS measurement, which yielded an SiO_2 value of 72 wt % despite basaltic soil in the APXS FOV (Ruff *et al.*, 2011). Finally, a Mini-TES observation of the dark-toned aeolian bedforms at the base of Pioneer Mound acquired on sol 1897 (Fig. 14C) was used as a way of contrasting its spectral features with those of the Pioneer Mound rocks. This material presumably is composed of basaltic sand with a variable dust cover similar to that seen in comparable settings elsewhere in the Columbia Hills (e.g., Arvidson *et al.*, 2008; Sullivan *et al.*, 2008). The standard mirror-dust correction also was applied to its Mini-TES spectrum. It is noteworthy that the Mini-TES observations of Pioneer Mound, Nancy Warren, and Stapledon include in the FOV some amount of basaltic sand and dust as well.

The spectra are shown in Fig. 15, from which it is apparent that a key feature of opal-A at $\sim 470\,cm^{-1}$ attributable to an Si-O bending mode (Lippincott *et al.*, 1958) is recognizable in the Pioneer Mound spectrum and clearly absent in the basaltic sand spectrum (purple spectrum). Additionally features throughout the spectra of the known opaline silica rocks observed after the sol 1220 dust build-up more closely resemble those of the Pioneer Mound spectrum than those of the basaltic sand spectrum. Thus, the combination of color, morphology and distribution, and TIR spectral characteristics of the Pioneer Mound rocks strongly supports the likelihood that they are composed of opaline silica.

Mounds with rocks composed of opaline silica are found in hydrothermal settings where hot springs build up sinter deposits around vent pools. Although hot spring vent mounds vary substantially in size and shape, examples from Puchuldiza and El Tatio are remarkably similar to Pioneer Mound in both size and shape (Fig. 16). The geomorphology of Pioneer Mound and evidence for opaline silica mineralogy are consistent with, although not uniquely interpretable as, an ancient hot spring vent mound. Geomorphically complete, hot spring vent mounds can still be recognized in ancient landscapes on Earth that hosted hydrothermal activity as far back as the Jurassic Age (Guido and Campbell, 2014).

5. Discussion

5.1. The origin of Home Plate silica

There is broad consensus in the literature that hydrothermal activity played a role in the origin of S-rich soils and opaline silica outcrops and soil in the vicinity of Home Plate. However, there has been a tendency to attribute the origin of these geological materials to a single hydrothermal process, despite the range of manifestations and processes known on Earth to result from an evolving hydrothermal system (c.f., Sillitoe, 2015). Given the disparities in composition, setting, physical properties, and location of the materials in the vicinity of Home Plate that are attributed to hydrothermal activity, it is reasonable to conclude that multiple hydrothermal processes likely were involved in their formation.

All Paso Robles class S-rich soils occur beneath a cover of minimally altered basaltic soil and have a composition that is reasonably interpreted to result from some combination of hydrothermal fluids and condensed volcanic vapors in an acid-sulfate fumarolic environment (Yen *et al.*, 2008). Such fluids also can lead to leaching of silicate rocks to produce opaline silica, but the stratiform outcrop expression of Home Plate opaline silica deposits and their sharp contacts with the underlying rocks are not characteristics of this process. In fact, leaching and alteration associated with fumarolic activity leads to polymineralic products with very irregular distributions, features evident at the small scale in Paso Robles soils (Ming *et al.*, 2008; Morris *et al.*, 2008) and at the larger scale among the fumaroles at Roosevelt Hot Springs (Fig. 4) and many other fumarolic settings on Earth. Sulfur Banks, Hawai'i is one such example cited by Squyres *et al.* (2008), yet its ragged, non-stratiform contacts and multiple alteration products (Fig. 17) are in stark contrast to the Home Plate opaline silica deposits.

The opaline silica outcrops and soil adjacent to Home Plate show no sulfur enrichment nor any alteration phases other than opal-A, with the exception of a possible halite crust in some places (Ruff and Farmer, 2016). We are not aware of any examples of halite-encrusted opaline silica produced in a fumarolic environment. Instead, the mineralogy, stratiform expression, and sharp contacts shown by the nodular silica outcrops are all recognized features of hot spring sinter deposits on Earth.

Sharp contacts and monomineralic composition are features of the sinter deposits at Roosevelt Hot Springs. One example is present on a hillside where sinter was deposited

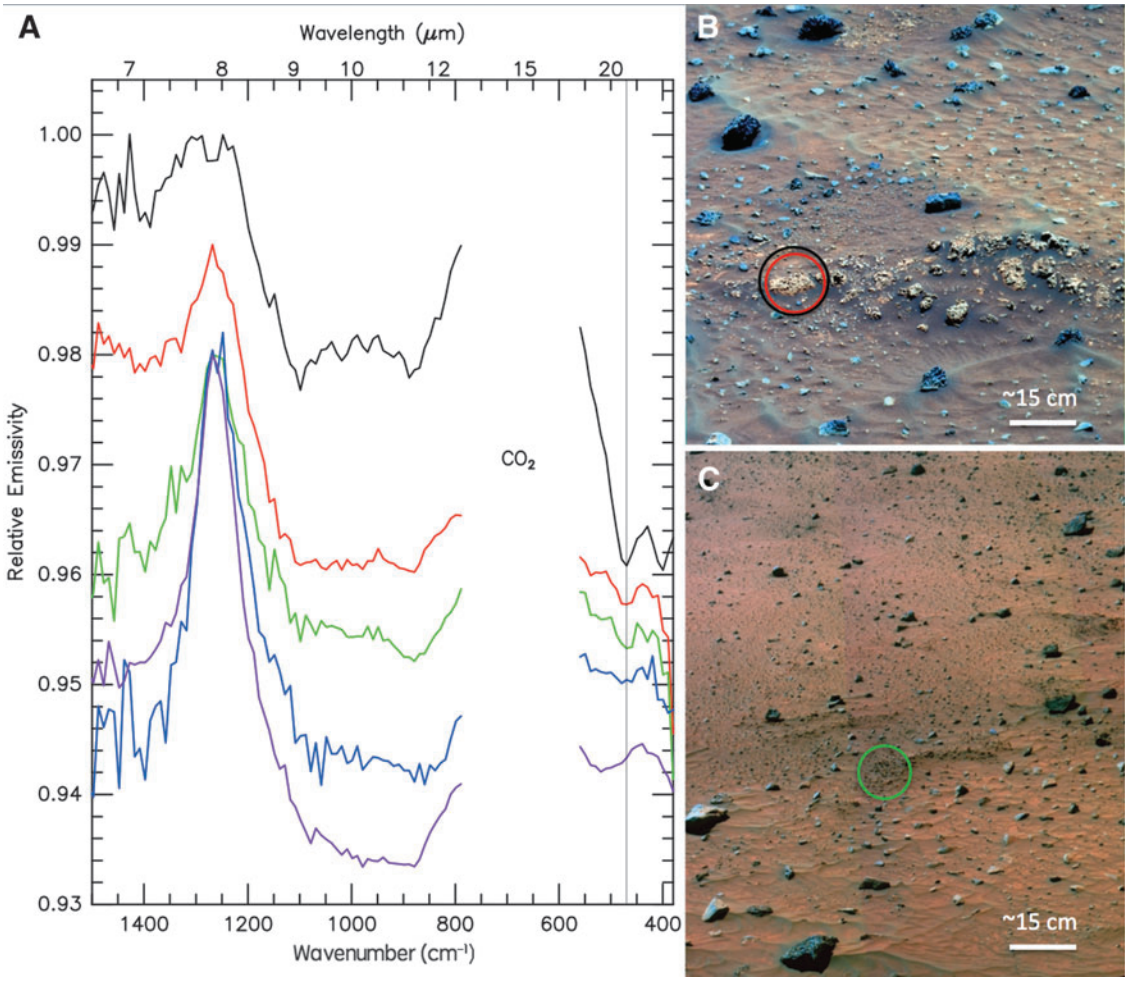

FIG. 15. Mini-TES spectra of known opaline silica rocks resemble that of Pioneer Mound. Color of spectra keyed to color of Mini-TES sample spots shown here and in Fig. 14B and C. **(A)** Spectra of opaline silica rock ''Nancy Warren'' were acquired before (black) and after (red) additional dust contamination of Mini-TES optics. The opaline silica outcrop ''Stapledon'' was observed after this contamination (green), as was Pioneer Mound (blue; Fig. 14B). Despite significant mirror-dust features, all contaminated spectra share the opaline silica feature at 470 cm^{-1} (vertical line) and similar features throughout; basaltic sand in front of Pioneer Mound does not (purple; Fig. 14C). **(B)** Nancy Warren with Mini-TES FOVs (Pancam false-color, sol 1190, P2534). **(C)** Stapledon with Mini-TES FOV (Pancam false-color, sol 1690, P2268).

in a discharge channel emanating from a former hot spring near the top of the hill shown in Fig. 4. The sinter deposit is now eroded into relief from the surrounding granitic alluvium that once hosted the channel, revealing the sharp contact at its base (Fig. 18). A smaller example from the Opal Mound location displays the now disaggregated remnants of sinter deposited on granitic regolith, revealing a sharp contact. The silica-rich fluids that deposited sinter also infiltrated the underlying regolith such that what was once loose particulate material is now cemented by opaline silica (Fig. 19), as shown by TIR spectroscopy (Supplementary Fig. S2). Common occurrences of granitic alluvium cemented by opaline silica were noted by Parry *et al.* (1980) throughout the Roosevelt Hot Springs/Opal Mound area, consistent with our example. This example of silicification due to hot spring fluids may be comparable to the candidate examples of silicification of Halley class rocks described in Section 4.3.

The exclusive contact relationship of nodular silica overlying Halley class rocks essentially precludes a stratigraphy in which silica was deposited after the emplacement and erosion of the volcaniclastic rocks and Irvine vesicular basalt/scoria in the vicinity of Home Plate (Fig. 11, model 2). If the silica was deposited as residue from fumarolic acid-sulfate leaching, it is highly unlikely to have been limited to a single rock unit in the stratigraphy (*i.e.*, Halley class). Steam and gases from fumaroles travel through host materials and, on exiting to the surface, drift with the wind and condense on any available surface. This produces an alteration that is independent of stratigraphy or topography (Fig. 17). Likewise, if the silica was emplaced as sinter deposits from hot spring or geyser discharge channels, it is highly unlikely to have been limited to just the Halley class rocks in a landscape littered with the eroded remnants of other rock units. Instead, the more likely scenario is one in which silica was emplaced stratigraphically on top of Halley class rocks before deposition of the overlying volcaniclastics and Irvine class rocks (Fig. 11, model 1). Both scenarios require subsequent erosion to re-expose the Halley class rocks, but only a conformable stratigraphic model (model 1)

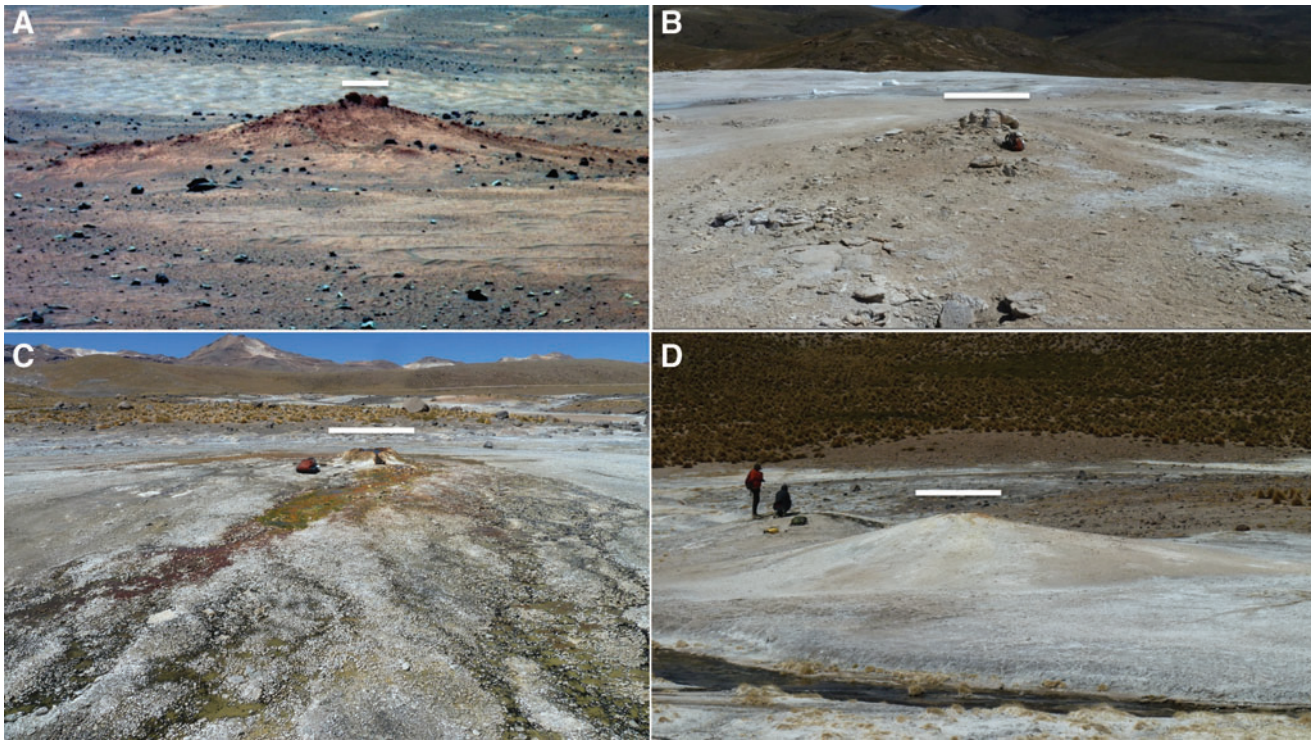

FIG. 16. Pioneer Mound resembles hot spring vent mounds of comparable size on Earth. White bar in each image represents ~2 m. **(A)** Pioneer Mound shown in Pancam false color image from sol 1860 (P2561). **(B)** Extinct hot spring mound at Puchuldiza, Chile. **(C)** Active hot spring mound with colorful microbial communities in discharge channels at El Tatio, Chile. **(D)** Active hot spring mound (discharge channel is on opposite side) at Puchuldiza, Chile.

FIG. 17. Fumarolic acid-sulfate leaching of basaltic materials at Sulfur Banks, Hawai'i. Alteration assemblage includes elemental S (yellow), sulfates (white), opaline silica (light gray), and Fe-oxides and oxyhydroxides (reddish hues). Neither stratigraphic or topographic control nor sharp contacts between altered and unaltered materials are evident.

FIG. 18. A topographically inverted sinter-filled discharge channel (arrows) from an extinct Roosevelt Hot Spring displays a sharp contact with the substrate. Yellow arrow points to view shown in the inset, where the hammer rests on granitic alluvium below the sinter deposit.

reasonably explains the presence of opaline silica rocks in contact with only one rock type.

Additionally, the morphology and texture of the Home Plate silica outcrops are a challenge to any kind of leaching origin. Leaching acts on existing rocks to produce opaline silica residue, a process not known to create nodular morphology, digitate structures, or breccia texture. Although subsequent erosional processes could have played a role in the formation of these features, our initial efforts with sandblasting suggest that erosion by wind-blown sand may not be an effective way to produce digitate structures. It may be even more difficult if aged opaline silica on Mars is comparable in hardness to aged sinter samples that we sandblasted, which proved to be surprisingly resistant to erosion. We are not aware of any examples of opaline silica residue on Earth manifesting the combination of morphologic and textural features displayed by Home Plate silica outcrops. Instead, all of these features are present, and indeed common, in hot spring sinter deposits on Earth.

It thus seems that the most straightforward explanation for the combination of hydrothermally derived materials in the Home Plate vicinity is a combination of hydrothermal processes manifested by fumaroles and hot springs and/or geysers. The S-rich soils are most consistent with acid-sulfate fumarolic activity, and the opaline silica outcrops are most consistent with alkali-chloride hot spring/geyser activity. These processes could have occurred simultaneously or sequentially, but most likely from the same hydrothermal system. Where S-rich soils show evidence for a silica component, as at the Arad and Tyrone locations (e.g., Wang *et al.*, 2008; Yen *et al.*, 2008; Rice *et al.*, 2010b) (Fig. 1), this could be an indication of one or both processes. For example, the Tyrone soil is several meters distant from a known occurrence of opaline silica outcrop (''Tyrone nodules''; Ruff *et al.*, 2011), so it could be a mixture of acid-sulfate altered soil and comminuted silica sinter. Elsewhere, there is evidence for overprinting of nodular silica by acidic alteration, as shown by the possible corrosion texture we identified on Elizabeth Mahon (Fig. 9), which may reflect the interaction of fumarolic gases after silica emplacement in a waning hydrothermal system.

Hydrothermal systems are known to undergo hydrologic changes as they wane, transitioning from hot spring/geyser activity to fumarolic activity (Drake *et al.*, 2014; cf. Campbell *et al.*, 2019), as shown, for example, at Roosevelt Hot Springs. Both can also occur at the same time in the same hydrothermal system, as shown, for example, at Yellowstone National Park (e.g., Fournier, 1989). Regardless of the evolution of the Home Plate hydrothermal system, it is reasonable to conclude from our observations that the opaline silica outcrops originated as sinter deposits from hot springs and/or geysers.

5.2. The significance of sinter on Mars

Opaline silica sinter deposits on Earth display morphologic and textural features related to temperature gradients,

FIG. 19. Cobbles and boulders of granitic regolith cemented by opaline silica near Opal Mound, Utah. Rectangle represents the inset view showing layer of sinter in sharp contact with the substrate. Blue rock hammer handle is ~20 cm long.

topography, evaporation rates, and associated microbial communities found in hot spring/geyser settings (e.g., Walter, 1976; Cady and Farmer, 1996; Jones *et al.*, 1998; Campbell *et al.*, 2001, 2015a). Facies models have been developed from such observations, but there are sufficient variations related to environmental factors and the particular characteristics of a given hydrothermal system that no single model is universally applicable. The hydrothermal fields of Chile's Altiplano are an example. They typically lack the distal, low-temperature marsh facies common in wetter environments (e.g., Campbell *et al.*, 2015a) and display morphological and textural variations in their sinter deposits that result from high evaporation/low precipitation rates (e.g., Nicolau *et al.*, 2014). Another example is the lack of broad sinter terraces at Roosevelt Hot Springs, which are otherwise common in long-lived hot spring systems with significant discharge volumes. However, features of vent, proximal slope, and channel facies are still recognizable there.

In this context, it is notable that the Home Plate silica deposits include rocks with breccia textures and digitate structures in separate locations, perhaps an indication of lateral and/or vertical facies variations. Walter (1976) described sinter breccia forming in the well-drained interfluves between discharge channels. Terrestrial examples of digitate structures that most closely resemble those on Mars occur in mid- to low-temperature portions of discharge channels. Thus, the presence of different textures and morphology among the silica outcrops could be an indication of at least two sinter facies in a possible hot spring/geyser setting at Home Plate. The unexplored Pioneer Mound structure, a candidate hot spring vent mound, would be an ideal place to search for evidence of additional sinter facies.

The concept of biomediated sinter facies is key to the possible significance of hot spring deposits on Mars. On Earth, morphologic, textural, and organic biosignatures are captured and preserved in sinter biofacies at macroscopic and microscopic scales (e.g., Cady and Farmer, 1996; Campbell *et al.*, 2015b; Jones *et al.*, 1998; Konhauser *et al.*, 2003; Teece *et al.*, 2020 in this issue; Walter *et al.*, 1996; White *et al.*, 1989). Sinter facies on Mars thus would offer multiple settings to search for biosignatures preserved in silica (e.g., Walter and Des Marais, 1993; Farmer and Des Marais, 1999; Campbell *et al.*, 2015a, 2015b; Westall *et al.*, 2015; Djokic *et al.*, 2017; Cady *et al.*, 2018). Although the digitate structures of some opaline silica nodules around Home Plate represent candidate biosignatures akin to those found in sinter biofacies on Earth (Ruff and Farmer, 2016), a singular focus on these features (McMahon *et al.*, 2018) is

insufficient to identify the origin of the silica deposits there. Instead, the rich set of observations presented herein provides robust evidence for sinter deposits at Home Plate.

6. Conclusions

A suite of observations summarized below supports the identification of a former hydrothermal system in the Home Plate region displaying multiple manifestations including both fumarolic and hot spring activity. The opaline silica rocks most likely are sinter deposits from hot spring/geyser activity, a key target in the search for potentially habitable environments and ancient life on Mars.

1. The presence of S-rich soils in the Columbia Hills is consistent with acid-sulfate fumarolic activity representing one manifestation of a hydrothermal system.
2. Opaline silica with nodular morphology and digitate structures similar to those shown by the silica deposits at Home Plate are common in hot spring and geyser discharge channels on Earth. Breccia textures evident among some Home Plate silica rocks are a common feature of hot spring/geyser sinter deposits. This combination of features is not recognized in leaching-derived opaline silica occurrences on Earth.
3. Outcrops of nodular opaline silica at Home Plate are stratiform in occurrence and in many places display sharp contacts with an underlying rock unit (Halley class). These characteristics are common among silica sinter deposits on Earth but are not recognized in fumarolic settings where silica residue is produced.
4. The exclusive contact relationship of nodular silica rocks on top of Halley class rocks favors their deposition before the emplacement of Home Plate, Low Ridge, and Mitcheltree Ridge volcaniclastic deposits and capping basaltic rocks.
5. A mound-shaped feature <50 m west of Home Plate named Pioneer Mound may represent a relatively intact ancient hot spring vent mound based on evidence for opaline silica rocks at this locale and morphology comparable to examples in Chile.

Acknowledgments

The authors thank the communities of Caspana and Toconce, Chile for allowing fieldwork and sample collection at El Tatio, and Rene Andrews of PacifiCorp for access to locations at Roosevelt Hot Springs. We appreciate the helpful comments of Greg Swayze and two anonymous reviewers.

Author Disclosure Statement

None of the authors has any commercial associations or financial interests that might create a conflict of interest in connection with this work.

Funding Information

S.W.R. and J.D.F. were supported with grants from the National Aeronautics and Space Administration Exobiology and Mars Data Analysis Programs. K.A.C. was supported by the Royal Society of New Zealand Marsden Fund and the Faculty Development Research Fund (Science Faculty, The University of Auckland). M.J.V.K. was supported by the Australian Research Council through Discovery Project No. DP180103204 and through the Centre of Excellence for Core to Crust Fluid Systems (CCFS) (www.ccfs.mq.edu.au). This is CCFS contribution No. 1362.

Supplementary Material

Supplementary Figure S1
Supplementary Figure S2

References

Allen, E.T. (1934) The agency of algae in the deposition of travertine and silica from thermal waters. *Am J Sci* 28: 373–389.

Arvidson, R.E., Ruff, S.W., Morris, R.V., Ming, D.W., Crumpler, L.S., Yen, A.S., Squyres, S.W., Sullivan, R.J., Bell, J.F., III, Cabrol, N.A., Clark, B.C., Farrand, W.H., Gellert, R., Greenberger, R., Grant, J.A., Guinness, E.A., Herkenhoff, K.E., Hurowitz, J.A., Johnson, J.R., Klingelhöfer, G., Lewis, K.W., Li, R., McCoy, T.J., Moersch, J., McSween, H.Y., Murchie, S.L., Schmidt, M., Schröder, C., Wang, A., Wiseman, S., Madsen, M.B., Goetz, W., and McLennan, S.M. (2008) Spirit Mars Rover mission to the Columbia Hills, Gusev Crater: mission overview and selected results from the Cumberland Ridge to Home Plate. J Geophys Res 113: E12S33.

Arvidson, R.E., Bell, J.F., III, Bellutta, P., Cabrol, N.A., Catalano, J.G., Cohen, J., Crumpler, L.S., Des Marais, D.J., Estlin, T., Farrand, W., Gellert, R., Grant, J.A., Greenberger, R.N., Guinness, E.A., Herkenhoff, K.E., Herman, J.A., Iagnemma, K.D., Johnson, J.R., Klingelhöfer, G., Li, R., Lichtenberg, K.A., Maxwell, S.A., Ming, D.W., Morris, R.V., Rice, M.S., Ruff, S.W., Shaw, A., Siebach, K.L., de Souza, P.A., Stroupe, A.W., Squyres, S.W., Sullivan, R.J., Talley, K.P., Townsend, J.A., Wang, A., Wright, J.R., and Yen, A.S. (2010) Spirit Mars Rover mission: overview and selected results from the northern Home Plate winter haven to the side of Scamander crater. *J Geophys Res* 115:E00F03.

Barbieri, R., Cavalazzi, B., Stifaletta, N., and Lopez-Garcia, P. (2014) Silicified biota in high-altitude, geothermally influenced ignimbrites at El Tatio Geyser Field, Andean Cordillera (Chile). *Geomicrobiol J* 31:493–508.

Bell, J.F., III, Joseph, J., Sohl-Dickstein, J.N., Arneson, H.M., Johnson, M.J., Lemmon, M.T., and Savransky, D. (2006) In-flight calibration and performance of the Mars Exploration Rover Panoramic Camera (Pancam) Instruments. *J Geophys Res* 111:E02S03.

Benson, C.A., Bizzoco, R.W., Lipson, D.A., and Kelley, S.T. (2011) Microbial diversity in nonsulfur, sulfur and iron geothermal steam vents. *FEMS Microbiol Ecol* 76:74–88.

Bethke, P.M., Rye, R.O., Stoffregen, R.E., and Vikre, P.G. (2005) Evolution of the magmatic-hydrothermal acid-sulfate system at Summitville, Colorado: integration of geological, stable-isotope, and fluid-inclusion evidence. *Chem Geol* 215: 281–315.

Bignall, G. and Browne, P.R.L. (1994) Surface hydrothermal alteration and evolution of the Te Kopia Thermal Area, New Zealand. *Geothermics* 23:645–658.

Cady, S.L. and Farmer, J.D. (1996) Fossilization processes in siliceous thermal springs: Trends in preservation along thermal gradients. In *Evolution of Hydrothermal Ecosystems on Earth (and Mars?)*, edited by G. Bock and J. Goodes, John Wiley and Sons, Chichester, pp 150–173.

Cady, S.L., Skok, J.R., Gulick, V.G., Berger, J.A., and Hinman, N.W. (2018) Chapter 7: Siliceous hot spring deposits: Why they remain key astrobiological targets. In *From Habitability to Life on Mars*, edited by N.A. Cabrol and E.A. Grins, Elsevier, Netherlands, pp 179–210.

Campbell, J.L., Gellert, R., Lee, M., Mallett, C.L., Maxwell, J.A., and O'Meara, J.M. (2008) Quantitative in situ determination of hydration of bright high-sulfate Martian soils. *J Geophys Res Planets* 113:E06S11.

Campbell, K.A., Sannazzaro, K., Rodgers, K.A., Herdianita, N.R., and Browne, P.R.L. (2001) Sedimentary facies and mineralogy of the Late Pleistocene Umukuri silica sinter, Taupo Volcanic Zone, New Zealand. *J Sediment Res* 71:728–747.

Campbell, K.A., Guido, D.M., Gautret, P., Foucher, F., Ramboz, C., and Westall, F. (2015a) Geyserite in hot-spring siliceous sinter: Window on Earth's hottest terrestrial (paleo)environment and its extreme life. *Earth Sci Rev* 148: 44–64.

Campbell, K.A., Lynne, B.Y., Handley, K.M., Sacha, J., Farmer, J.D., Guido, D.M., Foucher, F., Turner, S., and Perry, R.S. (2015b) Tracing biosignature preservation of geothermally silicified microbial textures into the geological record. *Astrobiology* 15:858–882.

Campbell, K.A., Guido, D.M., John, D.A., Vikre, P.G., Rhys, D., and Hamilton, A. (2019) The Miocene Atastra Creek sinter (Bodie Hills volcanic field, California and Nevada): 4D evolution of a geomorphically intact siliceous hot spring deposit. *J Volcanol Geotherm Res* 370:65–81.

Capuano, R.M. and Cole, D.R. (1982) Fluid-mineral equilibria in a hydrothermal system, Roosevelt Hot Springs, Utah. *Geochim Cosmochim Acta* 46:1353–1364.

Christensen, P.R., Jakosky, B.M., Kieffer, H.H., Malin, M.C., McSween Jr., H.Y., Nealson, K.H., Mehall, G.L., Silverman, S.H., Ferry, S., Caplinger, M., and Ravine, M. (2004) The Thermal Emission Imaging System (THEMIS) for the Mars 2001 Odyssey Mission. *Space Sci Rev* 110:85–130.

Clark, B.C., Arvidson, R.E., Gellert, R., Morris, R.V., Ming, D.W., Richter, L., Ruff, S.W., Michalski, J.R., Farrand, W.H., Yen, A.S., Herkenhoff, K.E., Li, R., Squyres, S.W., Schroder, C., Klingelhofer, G., and Bell, J.F., III. (2007) Evidence for montmorillonite or its compositional equivalent in Columbia Hills, Mars. *J Geophys Res* 112:E06S01.

Cockell, C.S., Harrison, J.P., Stevens, A.H., Payler, S.J., Hughes, S.S., Kobs Nawotniak, S.E., Brady, A.L., Elphic, R.C., Haberle, C.W., Sehlke, A., Beaton, K.H., Abercromby, A.F.J., Schwendner, P., Wadsworth, J., Landenmark, H., Cane, R., Dickinson, A.W., Nicholson, N., Perera, L., and Lim, D.S.S. (2019) A low-diversity microbiota inhabits extreme terrestrial basaltic terrains and their fumaroles: implications for the exploration of Mars. *Astrobiology* 19: 284–299.

Costello, E.K., Halloy, S.R.P., Reed, S.C., Sowell, P., and Schmidt, S.K. (2009) Fumarole-supported Islands of Biodiversity within a hyperarid, high-elevation landscape on Socompa Volcano, Puna de Atacama, Andes. *Appl Environ Microbiol* 75:735–747.

Day, A.L. and Allen, E.T. (1925) *The Volcanic Activity and Hot Springs of Lassen Peak*. Carnegie Institution of Washington, Washington, DC.

Djokic, T., Van Kranendonk, M.J., Campbell, K.A., Walter, M.R., and Ward, C.R. (2017) Earliest signs of life on land preserved in ca. 3.5 Ga hot spring deposits. *Nat Commun* 8:15263.

Drake, B.D., Campbell, K.A., Rowland, J.V., Guido, D.M., Browne, P.R.L., and Rae, A. (2014) Evolution of a dynamic paleo-hydrothermal system at Mangatete, Taupo Volcanic Zone, New Zealand. *J Volcanol Geotherm Res* 282:19–35.

Ellis, A.J. and Mahon, W.A.J. (1964) Natural hydrothermal systems and experimental hot-water/rock interactions. *Geochim Cosmochim Acta* 28:1323–1357.

Ellis, D.G., Bizzoco, R.W., and Kelley, S.T. (2008) Halophilic Archaea determined from geothermal steam vent aerosols. *Environ Microbiol* 10:1582–1590.

Farmer, J.D. and Des Marais, D.J. (1999) Exploring for a record of ancient Martian life. *J Geophys Res* 104:26977–26995.

Fournier, R.O. (1989) Geochemistry and Dynamics of the Yellowstone National Park Hydrothermal System. *Annu Rev Earth Planet Sci* 17:13–53.

Glennon, J.A. and Pfaff, R.M. (2003) The extraordinary thermal activity of El Tatio Geyser Field, Antofagasta Region, Chile. *GOSA Trans* 8:31–78.

Greeley, R., Leach, R.N., Williams, S.H., White, B.R., Pollack, J.B., Krinsley, D.H., and Marshall, J.R. (1982) Rate of wind abrasion on Mars. *J Geophys Res* 87:10,009–10,024.

Greeley, R., Foing, B.H., McSween Jr., H.Y., Neukum, G., Pinet, P., van Kan, M., Werner, S.C., Williams, D.A., and Zegers, T.E. (2005) Fluid lava flows in Gusev crater, Mars. *J Geophys Res* 110:E05008.

Guido, D.M., and Campbell, K.A. (2014) A large and complete Jurassic geothermal field at Claudia, Deseado Massif, Santa Cruz, Argentina. *J Volcanol Geotherm Res* 275:61–70.

Guido, D.M., Channing, A., Campbell, K.A., and Zamuner, A. (2010) Jurassic geothermal landscapes and fossil ecosystems at San Agustín, Patagonia, Argentina. *J Geol Soc* 167: 11–20.

Hamilton, A.R., Campbell, K.A., Rowland, J.V., Barker, S., and Guido, D. (2018) Characteristics and variations of sinters in the Coromandel Volcanic Zone: application to epithermal exploration AU—Hamilton, Ayrton R. *New Zeal J Geol Geophys* 1–19.

Haskin, L.A., Wang, A., Jolliff, B.L., McSween Jr., H.Y., Clark, B.C., Des Marais, D.J., McLennan, S.M., Tosca, N.J., Hurowitz, J.A., Farmer, J.D., Yen, A., Squyres, S.W., Arvidson, R.E., Klingelhöfer, G., Schröder, C., de Souza, P.A. Jr., Ming, D.W., Gellert, R., Zipfel, J., Brückner, J., Bell, J.F. 3rd., Herkenhoff, K., Christensen, P.R., Ruff, S., Blaney, D., Gorevan, S., Cabrol, N.A., Crumpler, L., Grant, J., and Soderblom, L. (2005) Water alteration of rocks and soils on Mars at the Spirit rover site in Gusev crater. *Nature* 436: 66–69.

Herdianita, N.R., Browne, P.R.L., Rodgers, K.A., and Campbell, K.A. (2000) Mineralogical and morphological changes accompanying ageing of siliceous sinter and silica residue. *Miner Depos* 35:48–62.

Hinman, N.W. and Walter, M.R. (2005) Textural Preservation in Siliceous Hot Spring Deposits During Early Diagenesis: examples from Yellowstone National Park and Nevada, U.S.A. *J Sediment Res* 75:200–215.

Hurowitz, J.A., McLennan, S.M., McSween Jr., H.Y., DeSouza Jr., P.A., and Klingelhöfer, G. (2006) Mixing relationships and the effects of secondary alteration in the Wishstone and Watchtower Classes of Husband Hill, Gusev Crater, Mars. *J Geophys Res* 111:E12S14.

Jones, B. and Renaut, R.W. (1997) Formation of silica oncoids around geysers and hot springs at El Tatio, northern Chile. *Sedimentology* 44:287–304.

Jones, B. and Renaut, R.W. (2003) Hot spring and geyser sinters: the integrated product of precipitation, replacement, and deposition. *Can J Earth Sci* 40:1549–1569.

Jones, B., Renaut, R.W., and Rosen, M.R. (1998) Microbial biofacies in hot-spring sinters; a model based on Ohaaki Pool, North Island, New Zealand. *J Sediment Res* 68:413–434.

Konhauser, K.O., Jones, B., Reysenbach, A.-L., and Renaut, R.W. (2003) Hot spring sinters: keys to understanding Earth's earliest life forms. *Can J Earth Sci* 40:1713–1724.

Kraft, M.D. and Greeley, R. (2000) Rock coatings and aeolian abrasion on Mars: application to the Pathfinder landing site. *J Geophys Res* 105:15,107–115,116.

Lewis, K.W., Aharonson, O., Grotzinger, J.P., Squyres, S.W., Bell, J.F., III, Crumpler, L.S., and Schmidt, M.E. (2008) Structure and stratigraphy of Home Plate from the Spirit Mars Exploration Rover. *J Geophys Res* 113:E12S36.

Lippincott, E.R., Van Valkenburg, A., Weir, C.E., and Bunting, E.N. (1958) Infrared studies on polymorphs of silicon dioxide and germanium dioxide. *J Res Natl Bur Stand* 61:61–70.

Lynne, B.Y. and Campbell, K.A. (2004) Morphologic and mineralogic transitions from opal-A to opal-CT in low-temperature siliceous sinter diagenesis, Taupo Volcanic Zone, New Zealand. *J Sediment Res* 74:561–579.

Lynne, B.Y., Campbell, K.A., Moore, J., and Browne, P.R.L. (2005) Diagenesis of 1900-year-old siliceous sinter (opal-A to quartz) at Opal Mound, Roosevelt Hot Springs, Utah, USA. *Sediment Geol* 179:249–278.

Lynne, B.Y., Campbell, K.A., James, B.J., Browne, P.R.L., and Moore, J. (2007) Tracking crystallinity in siliceous hot-spring deposits. *Am J Sci* 307:612–641.

Malin, M.C., Bell, J.F., III, Cantor, B.A., Caplinger, M.A., Calvin, W.M., Clancy, R.T., Edgett, K.S., Edwards, L., Haberle, R.M., James, P.B., Lee, S.W., Ravine, M.A., Thomas, P.C., and Wolff, M.J. (2007) Context Camera Investigation on board the Mars Reconnaissance Orbiter. *J Geophys Res Planets* 112:E05S04.

McEwen, A.S., Eliason, E.M., Bergstrom, J.W., Bridges, N.T., Hansen, C.J., Delamere, W.A., Grant, J.A., Gulick, V.C., Herkenhoff, K.E., Keszthelyi, L., Kirk, R.L., Mellon, M.T., Squyres, S.W., Thomas, N., and Weitz, C.M. (2007) Mars Reconnaissance Orbiter's High Resolution Imaging Science Experiment (HiRISE). *J Geophys Res Planets* 112: E05S02.

McHenry, L.J., Carson, G.L., Dixon, D.T., and Vickery, C.L. (2017) Secondary minerals associated with Lassen fumaroles and hot springs: implications for martian hydrothermal deposits. *Am Mineral* 102:1418–1434.

McMahon, S., Bosak, T., Grotzinger, J.P., Milliken, R.E., Summons, R.E., Daye, M., Newman, S.A., Fraeman, A., Williford, K.H., and Briggs, D.E.G. (2018) A field guide to finding fossils on Mars. *J Geophys Res Planets* 123:1012–1040.

McSween, H.Y., Ruff, S.W., Morris, R.V., Gellert, R., Klingelhofer, G., Christensen, P.R., McCoy, T.J., Ghosh, A., Moersch, J.E., Cohen, B.A., Rogers, A.D., Schröder, C., Squyres, S.W., Crisp, J., and Yen, A. (2008) Mineralogy of volcanic rocks in Gusev Crater, Mars: reconciling Mössbauer, Alpha Particle X-ray Spectrometer, and Miniature Thermal Emission Spectrometer spectra. *J Geophys Res* 113:E06S04.

Ming, D.W., Mittlefehldt, D.W., Morris, R.V., Golden, D.C., Gellert, R., Yen, A.S., Clark, B.C., Squyres, S.W., Farrand, W.H., Ruff, S.W., Ruff, S.W., Arvidson, R.E., Klingelhöfer, G., McSween, H.Y., Rodionov, D.S., Schröder, C., de Souza Jr., P.A., and Wang, A. (2006) Geochemical and mineralogical indicators for aqueous processes in the Columbia Hills of Gusev crater, Mars. *J Geophys Res* 111:E02S12.

Ming, D.W., Gellert, R., Morris, R.V., Arvidson, R.E., Bruckner, J., Clark, B.C., Cohen, B.A., d'Uston, C., Economou, T., Fleischer, I., Fleischer, I., Klingelhöfer, G., McCoy, T.J., Mittlefehldt, D.W., Schmidt, M.E., Schröder, C., Squyres, S.W., Tréguier, E., Yen, A.S., and Zipfel, J. (2008) Geochemical properties of rocks and soils in Gusev Crater, Mars: results of the Alpha Particle X-ray Spectrometer from cumberland ridge to Home Plate. *J Geophys Res* 113:E12S39.

Morris, R.V., Klingelhofer, G., Schroder, C., Fleischer, I., Ming, D.W., Yen, A.S., Gellert, R., Arvidson, R.E., Rodionov, D.S., Crumpler, L.S., Crumpler, L.S., Clark, B.C., Cohen, B.A., McCoy, T.J., Mittlefehldt, D.W., Schmidt, M.E., de Souza Jr., P.A., and Squyres S.W. (2008) Iron mineralogy and aqueous alteration from Husband Hill through Home Plate at Gusev Crater, Mars: results from the Mössbauer instrument on the Spirit Mars Exploration Rover. *J Geophys Res* 113:E12S42.

Morris, R.V., Ruff, S.W., Gellert, R., Ming, D.W., Arvidson, R.E., Clark, B.C., Golden, D.C., Siebach, K., Klingelhöfer, G., Schröder, C., Fleischer, I., Yen, A.S., and Squyres, S.W. (2010) Identification of carbonate-rich outcrops on Mars by the Spirit rover. *Science* 329:421–424.

Nicolau, C., Reich, M., and Lynne, B. (2014) Physico-chemical and environmental controls on siliceous sinter formation at the high-altitude El Tatio geothermal field, Chile. *J Volcanol Geotherm Res* 282:60–76.

Orange, F., Lalonde, S.V., and Konhauser, K.O. (2013) Experimental simulation of evaporation-driven silica sinter formation and microbial silicification in hot spring systems. *Astrobiology* 13:163–176.

Parry, W.T., Ballantyne, J.M., Bryant, N.L., and Dedolph, R.E. (1980) Geochemistry of hydrothermal alteration at the Roosevelt Hot Springs thermal area, Utah. *Geochim Cosmochim Acta* 44:95–102.

Payne, J.H. and Mau, K.T. (1946) A study of the chemical alteration of basalt in the Kilauea region of Hawaii. *J Geol* 54:345–358.

Rice, C.M., Ashcroft, W.A., Batten, D.J., Boyce, A.J., Caulfield, J.B.D., Fallick, A.E., Hole, M.J., Jones, E., Pearson, M.J., Rogers, G., Saxton, J.M., Stuart, F.M., Trewin, N.H., and Turner, G. (1995) A Devonian auriferous hot spring system, Rhynie, Scotland. *J Geol Soc* 152:229–250.

Rice, J.W.J., Greeley, R., Li, R., Wang, W., Crumpler, L., Farrand, W.H., and Team, A.S. (2010a) Geomorphology of the Columbia Hills complex: landslides, volcanic vent, and other Home Plates [abstract 2566]. In *41st Lunar and Planetary Science Conference*, Lunar and Planetary Institute, Houston.

Rice, M.S., Bell, J.F., III, Cloutis, E.A., Wang, A., Ruff, S.W., Craig, M.A., Baily, D.T., Johnson, J.R., de Souza Jr., P.A., and Farrand, W.H. (2010b) Silica-rich deposits and hydrated minerals at Gusev Crater, Mars: vis-NIR spectral characterization and regional mapping. *Icarus* 205:375–395.

Rodgers, K.A., Cook, K.L., Browne, P.R.L., and Campbell, K.A. (2002) The mineralogy, texture and significance of silica derived from alteration by steam condensate in three New Zealand geothermal fields. *Clay Miner* 37:299–322.

Rodgers, K.A., Browne, P.R.L., Buddle, T.F., Cook, K.L., Greatrex, R.A., Hampton, W.A., Herdianita, N.R., Holland, G.R., Lynne, B.Y., Martin, R., Newton, Z., Pastars, D., Sannazarro, K.L., and Teece, C.I.A. (2004) Silica phases in sinters and residues from geothermal fields of New Zealand. *Earth Sci Rev* 66:1–61.

Ruff, S.W. and Farmer, J.D. (2016) Silica deposits on Mars with features resembling hot spring biosignatures at El Tatio in Chile. *Nat Commun* 7:13554.

Ruff, S.W. and Hamilton, V.E. (2017) Wishstone to Watchtower: amorphous alteration of plagioclase-rich rocks in Gusev crater, Mars. *Am Mineral* 102:235–251.

Ruff, S.W., Christensen, P.R., Barbera, P.W., and Anderson, D.L. (1997) Quantitative thermal emission spectroscopy of minerals: a laboratory technique for measurement and calibration. *J Geophys Res Solid Earth* 102:14899–14913.

Ruff, S.W., Christensen, P.R., Blaney, D.L., Farrand, W.H., Johnson, J.R., Michalski, J.R., Moersch, J.E., Wright, S.P., and Squyres, S.W. (2006) The rocks of Gusev Crater as viewed by the Mini-TES instrument. *J Geophys Res* 111:E12S18.

Ruff, S.W., Farmer, J.D., Calvin, W.M., Herkenhoff, K.E., Johnson, J.R., Morris, R.V., Rice, M.S., Arvidson, R.E., Bell, J.F., III, Christensen, P.R., and Squyres, S.W. (2011) Characteristics, distribution, origin, and significance of opaline silica observed by the Spirit rover in Gusev crater, Mars. *J Geophys Res* 116:E00F23.

Ruff, S.W., Niles, P.B., Alfano, F., and Clarke, A.B. (2014) Evidence for a Noachian-aged ephemeral lake in Gusev crater, Mars. *Geology* 42:359–362.

Sanchez-Yanez, C., Reich, M., Leisen, M., Morata, D., and Barra, F. (2017) Geochemistry of metals and metalloids in siliceous sinter deposits: implications for elemental partitioning into silica phases. *Appl Geochem* 80:112–133.

Savransky, D. and Bell, J.F., III. (2004) True color and chromaticity of the Martian surface and sky from Mars Exploration Rover Pancam Observations [abstract P21A-0197]. In *Eos Trans. American Geophysical Union, Fall Meeting*, San Francisco.

Schinteie, R., Campbell, K.A., and Browne, P.R.L. (2007) Microfacies of stromatolitic sinter from acid-sulphate-chloride springs at Parariki Stream, Rotokawa geothermal field, New Zealand. *Paleontol Electron* 10:10.1.4A.

Schmidt, M.E., Ruff, S.W., McCoy, T.J., Farrand, W.H., Johnson, J.R., Gellert, R., Ming, D.W., Morris, R.V., Cabrol, N.A., Lewis, K.W., and Christian, S. (2008) Hydrothermal origin of halogens at Home Plate, Gusev Crater. *J Geophys Res* 113:E06S12.

Schmidt, M.E., Farrand, W.H., Johnson, J.R., Schroder, C., Hurowitz, J.A., McCoy, T.J., Ruff, S.W., Arvidson, R.E., Des Marais, D.J., Lewis, K.W., Ming, D.W., Squyres, S.W., and de Souza Jr., P.A. (2009) Spectral, mineralogical, and geochemical variations across Home Plate, Gusev Crater, Mars indicate high and low temperature alteration. *Earth Planet Sci Lett* 281:258–266.

Shinohara, H., Giggenbach, W.F., Kazahaya, K., and Hedenquist, J.W. (1993) Geochemistry of volcanic gases and hot springs of Satsuma-Iwojima, Japan: following Matsuo. *Geochem J* 27:271–285.

Sillitoe, R.H. (2015) Epithermal paleosurfaces. *Mineral Depos* 50:767–793.

Sillitoe, R.H. and Hedenquist, J.W. (2005) Linkages between Volcanotectonic Settings, Ore-Fluid Compositions, and Epithermal Precious Metal Deposits. In *Volcanic, Geothermal, and Ore-Forming Fluids: Rulers and Witnesses of Processes within the Earth*, edited by S.F. Simmons and I. Grahams, Society of Economic Geologists, Littleton, CO, pp 315–323.

Sorey, M.L., Suemnicht, G.A., Sturchio, N.C., and Nordquist, G.A. (1991) New evidence on the hydrothermal system in Long Valley caldera, California, from wells, fluid sampling, electrical geophysics, and age determinations of hot-spring deposits. *J Volcanol Geotherm Res* 48:229–263.

Squyres, S.W., Arvidson, R.E., Baumgartner, E.T., Bell, J.F., III, Christensen, P.R., Gorevan, S., Herkenhoff, K.E., Klingelhofer, G., Madsen, M.B., Morris, R.V., Rieder, R., and Romero, R.A. (2003) Athena Mars rover science investigation. *J Geophys Res* 108:8062.

Squyres, S.W., Arvidson, R.E., Bell, J.F., III, Bruckner, J., Cabrol, N.A., Calvin, W., Carr, M.H., Christensen, P.R., Clark, B.C., Crumpler, L.S., Des Marais, D.J., D'Uston, C., Economou, T., Farmer, J., Farrand, W., Folkner, W., Golombek, M., Gorevan, S., Grant, J.A., Greeley, R., Grotzinger, J., Haskin, L., Herkenhoff, K.E., Hviid, S., Johnson, J., Klingelhöfer, G., Knoll, A., Landis, G., Lemmon, M., Li, R., Madsen, M.B., Malin, M.C., McLennan, S.M., McSween, H.Y., Ming, D.W., Moersch, J., Morris, R.V., Parker, T., Rice Jr., J.W., Richter, L., Rieder, R., Sims, M., Smith, M., Smith, P., Soderblom, L.A., Sullivan, R., Wänke, H., Wdowiak, T., Wolff, M., and Yen, A. (2004) The Spirit Rover's Athena science investigation at Gusev Crater, Mars. *Science* 305:794–799.

Squyres, S.W., Arvidson, R.E., Blaney, D.L., Clark, B.C., Crumpler, L.S., Farrand, W.H., Gorevan, S., Herkenhoff, K.E., Hurowitz, J., Kusack, A., McSween, H.Y., Ming, D.W., Morris, R.V., Ruff, S.W., Wang, A., and Yen, A. (2006) The Rocks of the Columbia Hills. *J Geophys Res* 111:E02S11.

Squyres, S.W., Aharonson, O., Clark, B.C., Cohen, B.A., Crumpler, L.S., de Souza Jr., P.A., Farrand, W.H., Gellert, R., Grant, J.A., Grotzinger, J.P., Haldemann, A.F., Johnson, J.R., Klingelhöfer, G., Lewis, K.W., Li, R., McCoy, T.J., Mcewen, A.S., McSween, H.Y., Ming, D.W., Moore, J.M., Morris, R.V., Parker, T.J., Rice Jr., J.W., Ruff, S., Schmidt, M., Schroder, C., Soderblom, L.A., and Yen, A. (2007) Pyroclastic activity at Home Plate in Gusev Crater, Mars. *Science* 316:738–742.

Squyres, S.W., Arvidson, R.E., Ruff, S.W., Gellert, R., Morris, R.V., Ming, D.W., Crumpler, L.S., Farmer, J.D., Des Marais, D.J., Yen, A.S., McLennan, S.M., Calvin, W., Bell, J.F. 3rd, Clark, B.C., Wang, A., McCoy, T.J., Schmidt, M.E., and de Souza Jr., P.A. (2008) Detection of Silica-Rich Deposits on Mars. *Science* 320:1063–1067.

Sullivan, R., Arvidson, R., Bell, J.F., III, Gellert, R., Golombek, M., Greeley, R., Herkenhoff, K., Johnson, J., Thompson, S., Whelley, P., and Wray, J. (2008) Wind-driven particle mobility on Mars: insights from Mars Exploration Rover observations at ''El Dorado'' and surroundings at Gusev Crater. *J Geophys Res* 113:E06S07.

Tassi, F., Aguilera, F., Darrah, T., Vaselli, O., Capaccioni, B., Poreda, R.J., and Delgado Hertas, A. (2010) Fluid geochemistry of hydrothermal systems in the Arica-Parinacota, Tarapacá and Antofagasta regions (northern Chile). *J Volcanol Geotherm Res* 192:1–15.

Teece, B.L., George, S.C., Djokic, T., Campbell, K.A., Ruff, S.W., and Van Kranendonk, M.J. (2020) Biomolecules from fossilized hot-spring sinters: implications for the search for life on Mars. *Astrobiology* 20:537–551.

Tobler, D.J., Stefánsson, A., and Benning, L.G. (2008) In-situ grown silica sinters in Icelandic geothermal areas. *Geobiology* 6:481–502.

Tritlla, J., Camprubí, A., Morales-Ramírez, J.M., Iriondo, A., Corona-Esquivel, R., González-Partida, E., Levresse, G., and Carrillo-Chávez, A. (2004) The Ixtacamaxtitlán kaolinite deposit and sinter (Puebla State, Mexico): a magmatic-hydrothermal system telescoped by a shallow paleoaquifer. *Geofluids* 4: 329–340.

Truesdell, A.H., Nathenson, M., and Rye, R.O. (1977) The effects of subsurface boiling and dilution on the isotopic compositions of Yellowstone thermal waters. *J Geophys Res* 82:3694–3704.

Van Kranendonk, M.J. (2006) Volcanic degassing, hydrothermal circulation and the flourishing of early life on Earth: a review of the evidence from c. 3490–3240 Ma rocks of the Pilbara Supergroup, Pilbara Craton, Western Australia. *Earth Sci Rev* 74:197–240.

Van Kranendonk, M.J. and Pirajno, F. (2004) Geochemistry of metabasalts and hydrothermal alteration zones associated with c. 3.45 Ga chert and barite deposits: implications for the geological setting of the Warrawoona Group, Pilbara Craton, Australia. *Geochem Explor Environ, Analysis* 4:253–278.

Walter, M.R. (1976) Chapter 8.8 Hot-Spring Sediments in Yellowstone National Park. In *Developments in Sedimentology*, edited by M.R. Walters, Elsevier, Netherlands, pp 489–498.

Walter, M.R., Bauld, J., and Brock, T.D. (1972) Siliceous algal and bacterial stromatolites in hot spring and geyser effluents of Yellowstone National Park. *Science* 178:402–405.

Walter, M.R. and Des Marais, D.J. (1993) Preservation of biological information in thermal spring deposits: developing a strategy for the search for fossil life on Mars. *Icarus* 101:129–143.

Walter, M.R., Des Marais, D.J., Farmer, J.D., and Hinman, N.W. (1996) Lithofacies and biofacies of mid-Paleozoic thermal spring deposits in the Drummond Basin, Queensland, Australia. *Palaios* 11:497–518.

Wang, A., Bell, J.F., III, Li, R., Johnson, J.R., Farrand, W.H., Cloutis, E.A., Arvidson., R.E., Crumpler, L.S., Squyres, S.W., McLennan, S.M., Herkenhoff, K.E., Ruff, S.W., Knudson, A.T., Chen, W., and Greenberger, R. (2008) Light-toned salty soils and co-existing Si-rich species discovered by the Mars Exploration Rover Spirit in Columbia Hills. *J Geophys Res* 113:E12S40.

Weed, W.H. (1889) On the formation of siliceous sinter by vegetation of thermal springs. *Am J Sci* 37:351–359.

Westall, F., Foucher, F., Bost, N., Bertrand, M., Loizeau, D., Vago, J.L., Kminek, G., Gaboyer, F., Campbell, K.A., Breheret, J.G., Gautret, P., and Cockell, C.S. (2015) Biosignatures on Mars: what, Where, and How? Implications for the Search for Martian Life. *Astrobiology* 15:998–1029.

White, D.E. (1957) Thermal waters of volcanic origin. *Bull Geol Soc Am* 68:1637–1658.

White, D.E., Brannock, W.W., and Murata, K.J. (1956) Silica in hot-spring waters. *Geochim Cosmochim Acta* 10:17–59.

White, N.C., Wood, D.G., and Lee, M.C. (1989) Epithermal sinters of Paleozoic age in north Queensland, Australia. *Geology* 17:718–722.

Winchell, K., and Rice, M.S. (2017) Characterizing the extent of hydrothermal activity in Gusev crater, Mars. *Geol Soc Am Abstracts* 49:277-6.

Yen, A.S., Morris, R.V., Clark, B.C., Gellert, R., Knudsen, A.T., Squyres, S.W., Mittlefehldt, D.W., Ming, D.W., Arvidson, R., McCoy, T., Schmidt, M., Hurowitz, J., Li, R., and Johnson, J.R. (2008) Hydrothermal processes at Gusev Crater: an evaluation of Paso Robles class soils. *J Geophys Res* 113:E06S10.

Yen, A.S., Gellert, R., Berger, J.A., Clark, B.C., Cohen, B.A., Ming, D.W., Mittlefehldt, D.W., O'Connell-Cooper, C.D., Schmidt, M.E., Thompson, L.M., and VanBommel, S.J. (2019) Understanding Martian alteration processes by comparing in-situ chemical measurements from multiple landing sites [abstract 2089]. In *Ninth International Conference on Mars*, Pasadena, CA.

Address correspondence to:
Steven W. Ruff
School of Earth and Space Exploration
Arizona State University
Mars Space Flight Facility
Moeur Building Room 131
Tempe, AZ 85287-6305

E-mail: steve.ruff@asu.edu

Submitted 31 January 2019
Accepted 11 September 2019
Associate Editor: Jack Mustard

Abbreviations Used

APXS = Alpha Particle X-ray Spectrometer
CTX = Context Camera
EM = Elizabeth Mahon
FOV = field of view
GW = Gertrude Weise
HiRISE = High-Resolution Imaging Science Experiment
HP = Home Plate feature
HPc = Home Plate-like deposits
MI = Microscopic Imager
Mini-TES = Miniature Thermal Emission Spectrometer
MM = Milltown Malbay
MR = Mitcheltree Ridge
MRO = Mars Reconnaissance Orbiter
NL = Norma Luker
NW = Nancy Warren
opal-A = amorphous opal phase
THEMIS VIS = Thermal Emission Imaging System Visible Imaging System
TIR = thermal infrared